

AO-A193 899

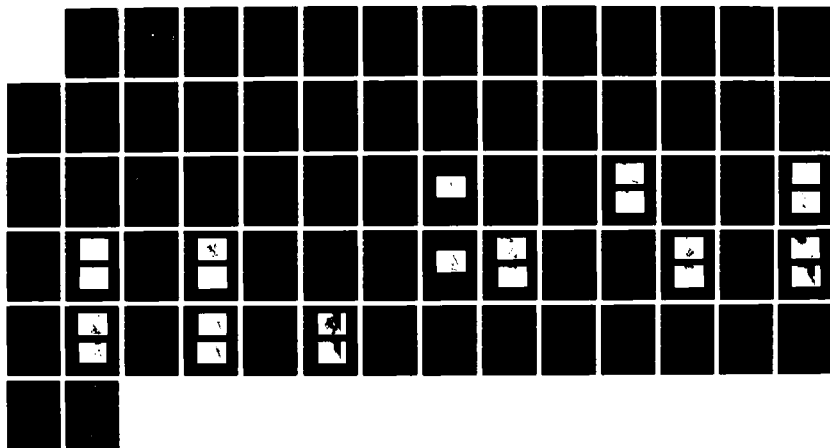
STRATOCUMULUS AND CLOUD-FREE REFLECTANCE FROM
MULTI-SPECTRAL SATELLITE MEASUREMENTS(U) NAVAL
POSTGRADUATE SCHOOL MONTEREY CA F M TETTELBACH DEC 87

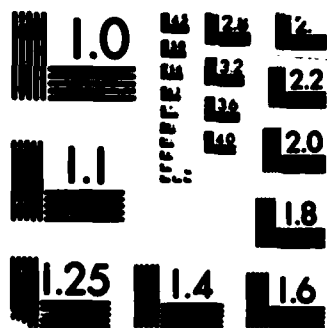
1/1

UNCLASSIFIED

F/G 28/6

NL





MICROCOPY RESOLUTION TEST CHART
... STANDARD 1963-A

DTIC FILE COP: (2)

NAVAL POSTGRADUATE SCHOOL

Monterey, California

AD-A193 899



DTIC
ELE
JUN 03 1988
H

THESIS

STRATOCUMULUS AND CLOUD-FREE
REFLECTANCE
FROM MULTI-SPECTRAL SATELLITE
MEASUREMENTS

by

Fredrick M. Tettelbach, Jr.

December 1987

Thesis Advisor

Philip A. Durkee

Approved for public release; distribution is unlimited.

88 6 1 115

8a NAME OF FUNDING: SPONSORING ORGANIZATION		8d OFFICE SYMBOL (if applicable)		9 PROCUREMENT INSTRUMENT IDENTIFICATION NUMBER			
8c ADDRESS (City, State, and ZIP Code)				10 SOURCE OF FUNDING NUMBERS			
		PROGRAM ELEMENT NO	PROJECT NO	TASK NO	WORK UNIT ACCESSION NO		
11 TITLE (Include Security Classification) STRATOCUMULUS AND CLOUD-FREE REFLECTANCE FROM MULTI-SPECTRAL SATELLITE MEASUREMENTS							
12 PERSONAL AUTHOR(S) Tettelbach, Fredrick M., Jr.							
13a TYPE OF REPORT Master's Thesis		13b TIME COVERED FROM TO		14 DATE OF REPORT (Year, Month, Day) 1987 December		15 PAGE COUNT 69	
16 SUPPLEMENTARY NOTATION							
17 COSATI CODES			18 SUBJECT TERMS (Continue on reverse if necessary and identify by block number)				
FIELD	GROUP	SUB-GROUP	satellite cloud analysis, cloud distribution, aerosol distribution, cloud microphysics,				
			-69 50 15				
19 ABSTRACT (Continue on reverse if necessary and identify by block number) A summary of the multi-spectral radiative characteristics of marine stratocumulus clouds and pre-cloud suspended aerosols was compiled for August 1986 over the offshore regions of the North American west coast. NOAA-9 AVHRR data were utilized at Channel 1 visible (0.63 μm), Channel 2 red visible/near infrared (0.90 μm), Channel 3 near infrared (3.7 μm), and Channel 4 thermal infrared (11.0 μm) wavelengths. Stratus cloud pixels and cloud-free area pixels were identified within the data set, and average radiation parameters with associated standard deviations were calculated for the two pixel classifications. The Channel 3 radiance values were reduced to reflectances through a unique procedure that removed the emittance from the total radiance using the detected Channel 4 emittance. Additionally, radiance ratios were determined that compared Channel 1 to Channel 2 reflectances and Channel 1 to Channel 3							

reflectances. Significant results included a concentration of high cloud-free Channel 1/Channel 2 reflectance ratios (greater than 1.70) along the entire continental coast, implying the presence of a large number of smaller (less than 1 μ m, continental-like) suspended aerosols relative to aerosols over the Pacific Ocean with reflectance ratios less than 1.60 (marine-like). Stratocumulus cloud characteristics were derived from the cloud Channel 1/Channel 3 reflectance ratios. Lower ratios implied relatively thin, dry stratus with a low liquid water content (low Channel 1 reflectance) and a greater number of smaller cloud droplets (high Channel 3 reflectance). Low reflectance ratios (less than 2.50) were observed for stratus generally in the same location and downwind of continental-like aerosols. A distinct correlation exists between the aerosols acting as CCN and the stratus that develops along the coast. Observations of sea surface temperatures (SST), coastal clearing, and stratus persistence and coverage are also described.



"Original contains color plates: All information herein will be in black and white"

Accession For	
NTIS GRA&I	<input checked="" type="checkbox"/>
DTIC TAB	<input type="checkbox"/>
Unannounced	<input type="checkbox"/>
Justification _____	
By _____	
Distribution/ _____	
Availability Codes	
Dist	Avail and/or Special
A-1	

Approved for public release; distribution is unlimited.

Stratocumulus and Cloud-free Reflectance
From Multi-spectral Satellite Measurements

by

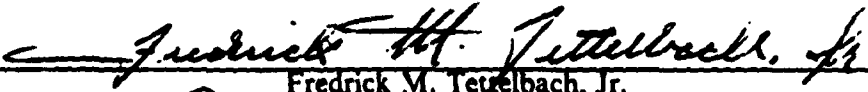
Fredrick M. Tettelbach, Jr.
Lieutenant, United States Navy
B.S., United States Naval Academy, 1981

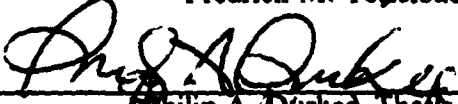
Submitted in partial fulfillment of the
requirements for the degree of

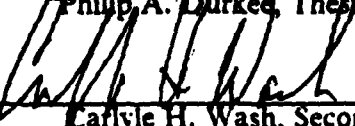
MASTER OF SCIENCE IN METEOROLOGY AND OCEANOGRAPHY

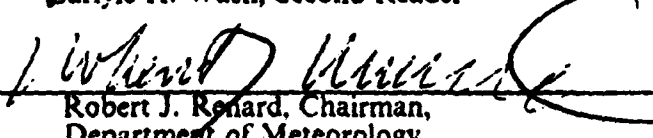
from the


NAVAL POSTGRADUATE SCHOOL
December 1987

Author: 
Fredrick M. Tettelbach, Jr.

Approved by: 
Philip A. Durkee, Thesis Advisor


Carlyle H. Wash, Second Reader


Robert J. Renard, Chairman,
Department of Meteorology


Gordon E. Schacher,
Dean of Science and Engineering

ABSTRACT

A summary of the multi-spectral radiative characteristics of marine stratocumulus clouds and pre-cloud suspended aerosols was compiled for August 1986 over the offshore regions of the North American west coast. NOAA-9 AVHRR data were utilized at Channel 1 visible (0.63 μm), Channel 2 red visible/near infrared (0.90 μm), Channel 3 near infrared (3.7 μm), and Channel 4 thermal infrared (11.0 μm) wavelengths. Stratus cloud pixels and cloud-free area pixels were identified within the data set, and average radiation parameters with associated standard deviations were calculated for the two pixel classifications. The Channel 3 radiance values were reduced to reflectances through a unique procedure that removed the emittance from the total radiance using the detected Channel 4 emittance. Additionally, radiance ratios were determined that compared Channel 1 to Channel 2 reflectances and Channel 1 to Channel 3 reflectances. Significant results included a concentration of high cloud-free Channel 1:Channel 2 reflectance ratios (greater than 1.70) along the entire continental coast, implying the presence of a large number of smaller (less than 1 μm , continental-like) suspended aerosols relative to aerosols over the Pacific Ocean with reflectance ratios less than 1.60 (marine-like). Stratocumulus cloud characteristics were derived from the cloud Channel 1:Channel 3 reflectances ratios. Lower ratios implied relatively thin, dry stratus with a low liquid water content (low Channel 1 reflectance) and a greater number of smaller cloud droplets (high Channel 3 reflectance). Low reflectance ratios (less than 2.50) were observed for stratus generally in the same location and downwind of continental-like aerosols. A distinct correlation exists between the aerosols acting as CCN and the stratus that develops along the coast. Observations of sea surface temperatures (SST), coastal clearing, and stratus persistence and coverage are also described.

TABLE OF CONTENTS

I.	INTRODUCTION	10
	A. MOTIVATION	10
	B. OBJECTIVES	11
	C. ORGANIZATION	12
II.	THEORY	13
	A. ELECTROMAGNETIC SPECTRUM	13
	B. RADIATIVE PROCESSES	14
	1. Channel 1	17
	2. Channel 2	19
	3. Channel 3	19
	4. Channel 4	20
	C. MULTI-SPECTRAL RELATIONSHIPS	21
	1. Channel 1/Channel 2 Ratio	22
	2. Channel 1/Channel 3 Ratio	22
III.	DATA ANALYSIS	24
	A. DATA DESCRIPTION	24
	B. DATA PROCESSING	25
IV.	RESULTS	32
	A. CLOUD-FREE CASES	32
	1. Pixel Counts	32
	2. Channel 1 Reflectances	35
	3. Channel 1/Channel 2 Reflectance Ratios	38
	4. Channel 4 Temperatures	40
	B. STRATOCUMULUS CLOUD CASES	44
	1. Pixel Counts	44
	2. Channel 1 Reflectances	46
	3. Channel 1/Channel 2 Reflectance Ratios	50

4.	Channel 3 Reflectances	52
5.	Channel 1 Channel 3 Reflectance Ratios	56
6.	Channel 4 Temperatures	58
V.	CONCLUSION	61
A.	SUMMARY	61
B.	RECOMMENDATIONS	63
	LIST OF REFERENCES	65
	INITIAL DISTRIBUTION LIST	67

LIST OF TABLES

1. AVHRR CHANNEL WAVELENGTHS 16

LIST OF FIGURES

2.1	Absorptance spectrum for the earth's atmospheric gases, from Fleagle and Businger (1980)	15
3.1	Summary area	26
3.2	Sun-earth-satellite geometry	28
4.1	Cloud-free pixel counts	33
4.2a	Cloud-free channel 1 reflectances	36
4.2b	Cloud-free channel 1 standard deviations	36
4.3a	Cloud-free channel 2 reflectances	39
4.3b	Cloud-free channel 2 standard deviations	39
4.4a	Cloud-free channel 1/channel 2 reflectance ratios (x 100)	41
4.4b	Cloud-free channel 1/channel 2 ratio standard deviations	41
4.5a	Cloud-free channel 4 temperatures	43
4.5b	Cloud-free channel 4 standard deviations	43
4.6	NWS monthly mean SST for August 1986 (1.0°C interval), from Dept. of Commerce, NOAA (1986)	45
4.7	Stratus pixel counts	47
4.8a	Stratus channel 1 reflectances	48
4.8b	Stratus channel 1 standard deviations	48
4.9a	Stratus channel 2 reflectances	51
4.9b	Stratus channel 2 standard deviations	51
4.10a	Stratus channel 1/channel 2 reflectance ratios (x 100)	53
4.10b	Stratus channel 1/channel 2 ratio standard deviations	53
4.11a	Stratus channel 3 reflectances	55
4.11b	Stratus channel 3 standard deviations	55
4.12a	Stratus channel 1/channel 3 reflectances ratios (x 100)	57
4.12b	Stratus channel 1/channel 3 ratio standard deviations	57
4.13a	Stratus channel 4 temperatures	59
4.13b	Stratus channel 4 standard deviations	59

ACKNOWLEDGEMENTS

I would like to thank Mr. Doug Burks of the Naval Postgraduate School Meteorology Department for his programming and problem-solving assistance. Mr. Burks wrote the software for the data calibration and navigation, and he assisted with the graphics-interfacing software used to generate the images presented in this study. Mr. Rick Kohrs of the Naval Postgraduate School Meteorology Department was very helpful with the time-consuming task of processing the data and producing the graphic images. Dr. Carlyle H. Wash carefully reviewed the manuscript and contributed significant scientific input and literary criticism. I must especially thank Dr. Philip A. Durkee for his patience and encouragement throughout this thesis work, in addition to his instruction and guidance.

I. INTRODUCTION

Satellites are utilized to detect radiation, backscattered and emitted, from the earth's surface and atmosphere in narrow and separate wavelength bands of the electromagnetic spectrum. Atmospheric elements such as suspended aerosols and the various types of clouds interact differently with the electromagnetic energy within each wavelength band, thus creating unique radiation patterns and values for satellite detection. The scattering and absorption characteristics of these elements are responsible for the distinctive radiances. Therefore, information about the identifiable atmospheric features can be inferred from a careful examination of these radiances. Additional aerosol and cloud characteristics can be derived from comparisons, in the form of ratios, of the different reflectances measured in each wavelength band. A correlation between marine stratocumulus clouds and pre-cloud aerosols can be developed through such reflectance ratios.

Satellites such as the NOAA-9 provide high resolution data over a large area each day. It is an ideal platform for collecting data to be compiled in a temporal summary that includes a broad spectrum of radiation measurements over a defined, but fairly large, region. By creating a composite summary over a single month, relatively persistent and significant features can be identified with some climatological implications. Utilizing the different reflectance and emittance values of individual atmospheric elements within distinct wavelength bands, certain elements can be recognized and separated from other features and the earth's surface. Thus, a summary of a specific feature can be created to include only the radiative characteristics of that particular element. This research compiled such summaries for marine stratocumulus clouds and cloud-free oceanic areas.

A. MOTIVATION

A monthly radiance summary such as this provides a basis for long term and long range decision-making, planning and calculations. There are two major motivations for this type of data analysis and its examination of the multi-spectral radiative characteristics of both cloud-free and cloud conditions in the atmosphere. They are separated into a military application and a climate application.

From a military perspective, the complex sensing systems of many smart weapons today enable them to transit over the horizon, then locate and strike targets. However, these systems are also sensitive to environmental factors. Some systems are critically affected by variations in the electro-optical properties of the atmosphere and atmospheric elements like clouds. Low-level trajectories make these weapons especially susceptible to the effects of suspended aerosols and stratocumulus clouds. Knowledge of the characteristics and locations of such features can be vital to determining the sensor settings, weapon paths, and launch no launch criteria. A monthly summary is obviously not as useful as real time *in situ* data in most situations, but the long range capability of many weapon systems requires information over a large area and at very distant locations. These data will likely be sparse, if available, and climatological data including such a summary and or satellite data, for which the summary would provide useful interpretation assistance, will be the environmentalist's tools for decision-making. Weapon systems with pre-planned missions, specifically the Tomahawk cruise missile which is highly sensitive to electro-optical properties, would require these data to improve its success percentage.

From a climatic perspective, this type of information is important to estimations of the earth's radiation budget. Coakley *et al.* (1987) specifically noted the radiation effects of suspended aerosols through the scattering and absorption of solar radiation, and their influence on the radiative characteristics of clouds that can form from these aerosols. It was found that aerosol variations can result in strong cloud reflectance variations. The influence of these aerosols on the radiation budget through these clouds could be much greater than the effects of the aerosols themselves. Specifically, man-made or urban aerosols, since they are often suspended in the atmosphere in high concentrations, increase the near infrared cloud reflectance so that a radiation decrease occurs at the earth's surface. If man-made aerosols increased in number along with the expected carbon dioxide (CO₂) increase, the reduction of incident solar radiation would work in the opposite direction of the warming trend of CO₂ through the 'Greenhouse effect' and may be the same order of magnitude. Such an effect on the earth's radiation budget will have a major impact on climate.

B. OBJECTIVES

The purpose of this study is to create a composite summary for August 1986 of the multi-spectral radiative characteristics of the cloud-free ocean and marine stratocumulus clouds off the western coast of the United States. The analyses are

composed of NOAA-9 satellite data in the visible, near infrared, and infrared portions of the electromagnetic spectrum utilizing the various channels of the Advanced Very High Resolution Radiometer (AVHRR). The summary includes average reflectance at multiple wavelengths, average temperature (sea-surface or cloud-top), and a spectral ratio of reflectances.

An additional objective is to identify significant features in these different analyses. Specifically, this study will concentrate on pre-cloud aerosol information derived from visible visible-near infrared ratios in cloud-free conditions to provide particle number, composition and size distribution characteristics (Durkee, 1987). Another consideration will be stratus cloud visible infrared ratios for absorption and size distribution information (Twomey, 1977). Theoretically, some correlation is drawn between the suspended aerosols and the stratus cloud characteristics. Additional information derived from infrared measurements to include sea-surface temperatures in cloud-free cases and cloud-top heights from stratus cloud cases.

The final objective is to develop plausible explanations for these features. This will be accomplished through examination of the theoretical and physical basis of atmospheric attenuation, the climatology for late summer in this ocean region, the synoptic-scale analyses for the selected dates, and other studies and papers on specific subjects related to this summary.

C. ORGANIZATION

The theoretical background for this study is described in Chapter II. First, the electromagnetic spectrum is discussed with its wavelength-dependent atmospheric attenuation characteristics. The particle size to wavelength relationship of scattering classifications is highlighted, followed by the absorption spectrum of solar radiation by atmospheric gases. Then, each AVHRR channel and channel ratio will be discussed in terms of its wavelength band and the associated radiative effects of molecular gases, suspended aerosols, clouds and the surface.

Chapter III concentrates on a description of the data set and the procedure for processing these data. Included in the procedure are significant details covering the calculations of the reflectances, specifically the Channel 3 reflectance, and the temperatures from thermal emissions. The Chapter IV contains a description of the results, divided by cloud-free cases and stratus cloud cases. Each computed channel and channel ratio will be examined with explanations or suggestions developed for the important features. Chapter V summarizes the results of this thesis. Recommendations improvements and future studies are also included.

II. THEORY

A. ELECTROMAGNETIC SPECTRUM

Electromagnetic energy propagates through space and the earth's atmosphere in small packets called photons. Electromagnetic radiant energy is then represented by a stream of photons with propagation velocity (c) and an oscillation frequency (f). The electromagnetic radiation then can be classified by a characteristic wavelength ($\lambda = c/f$). The distribution of electromagnetic energy as a function of wavelength makes up the electromagnetic spectrum. Significant wavelength regions for satellite detection of this energy include the visible at 0.3 to 0.7 μm , the near infrared at 0.8 to 5.0 μm , and the thermal infrared at 5.0 to 20.0 μm .

The theoretical development of atmospheric attenuation is described in Liou (1980), and the general principles are presented. Radiation propagating through the earth's lower atmosphere is attenuated by interactions with gaseous molecules, suspended aerosols, clouds and the earth's surface. This attenuation occurs in two basic forms; scattering and absorption. Scattering consists of any physical process in which the electromagnetic energy of a photon is redirected in different directions as a result of an interaction with a particle. These processes include the reflection, refraction, or diffraction. The measured reflectance includes the detection of these scattering events that produce exiting photons in the direction of the satellite sensor.

Scattering is heavily wavelength and scattering element size dependent. The relationship of these two factors defines the type of scattering that will occur at each interaction. The element composition and shape are also important scattering factors, but are secondary to the size relationship. Rayleigh scattering occurs when the wavelength of the incident radiation is much greater than the size of the scattering matter ($r \ll \lambda$). The scattering pattern is often referred to as 'peanut-shaped', where the scattering is concentrated equally in forward and back lobes along the incident path. The intensity of this type of scattering is proportional to the inverse fourth power of the incident wavelength ($\propto \lambda^{-4}$). The Mie scattering solution is based upon the assumption that the scattering element is spherically shaped, which is approximate for water droplets. This type of scattering occurs when the incident wavelength of energy approximates the size of the scattering matter ($r \sim \lambda$). As the wavelength to

element size relationship approaches the Mie solution from the Rayleigh solution, the scattering pattern becomes increasingly concentrated in the forward lobe at the expense of the back lobe. Therefore, the Mie solution is anisotropic or forward-scattering. When the element size is much greater than the incident wavelength of energy, the scattering is characterized as geometric and follows the principles of ray optics ($r \gg \lambda$). The scattering pattern also becomes less wavelength-dependent. Other important factors to the scattering solutions, especially for Mie scattering, are the particle's chemical composition, size distribution, and vertical distribution in the atmosphere.

Incident electromagnetic energy also may be attenuated through absorption of photons by atmospheric and surface elements. This absorption is dependent upon the incident energy wavelength and chemical nature of the matter. The absorptance spectrum of the earth's atmospheric gases is depicted in Fig. 2.1. Strong absorbers of radiant energy are also strong emitters of this energy at given wavelengths according to Kirchoff's law.

Close inspection of Fig. 2.1 reveals that in certain wavelength regions there is little or no absorption by atmospheric gases. These absorption wavelength bands are called atmospheric or absorption windows. One of the sensors on the NOAA-9 satellite is the Advanced Very High Resolution Radiometer (AVHRR), which measures backscattered and emitted radiation in five of these windows. The five AVHRR channels and their respective wavelength detection bands are listed in Table 1 (Kidwell, 1986). The thermal emittance measurements from channel 5 were not utilized in this thesis.

B. RADIATIVE PROCESSES

Information about atmospheric and surface features can be derived from the backscattered and emitted radiance measured by the AVHRR. Since each channel detects this radiant energy in a separate wavelength band, different characteristics of these features will be revealed based on the scattering properties. Suspended aerosol quantities and size distributions along with several cloud characteristics, especially the thickness and liquid water content, are revealed by the visible wavelength measurements of channel 1 and channel 2 (Durkee, 1987 and Twomey, 1977). Different cloud properties, such as the number of droplets and their size distributions inferred from cloud condensation nuclei (CCN) characteristics become more representative of the radiance received in the longer near infrared wavelengths by channel 3. The thermal infrared wavelengths detected by channel 4 provide an

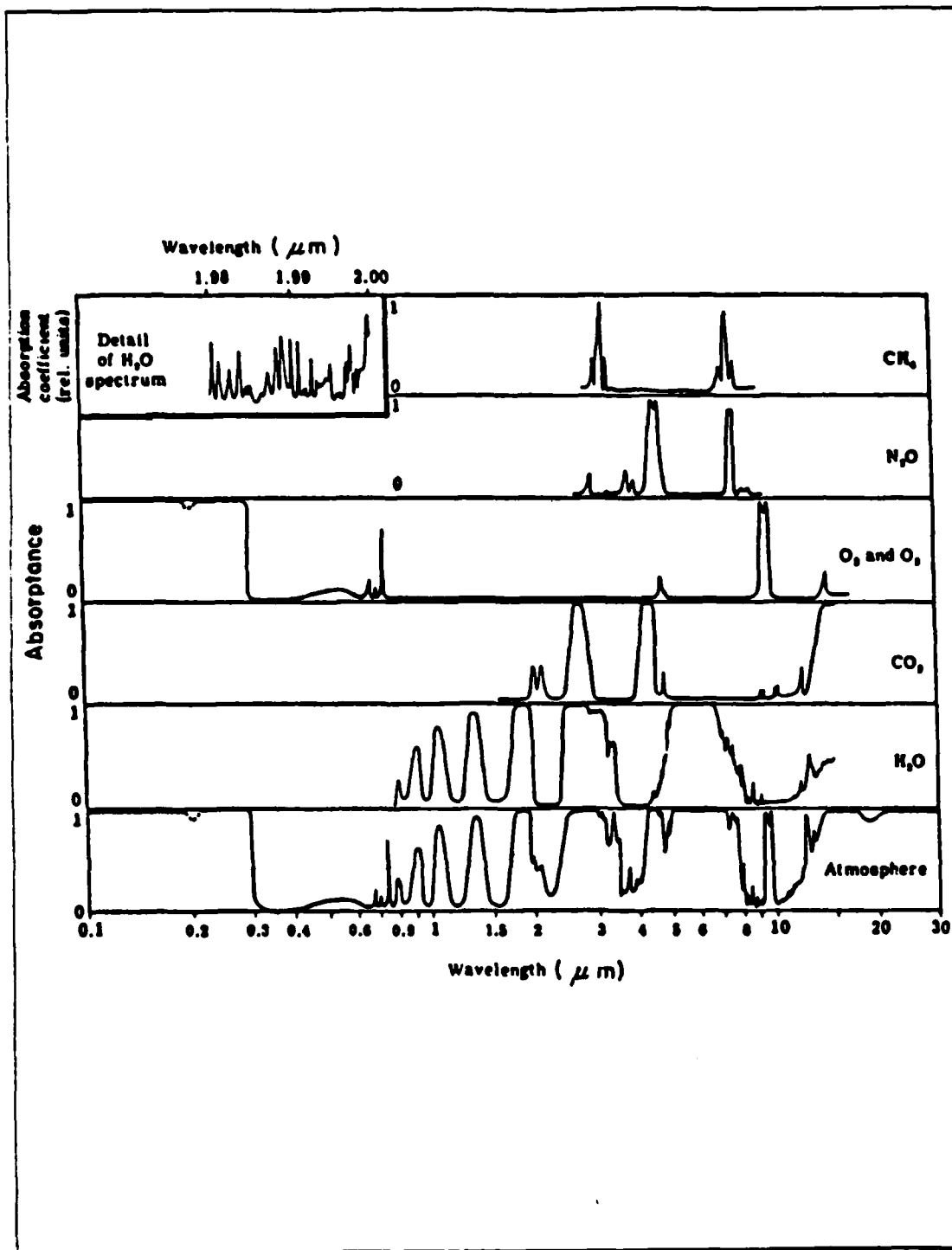


Fig. 2.1 Absorptance spectrum for the earth's atmospheric gases, from Fleagle and Businger (1980).

TABLE 1
AVHRR CHANNEL WAVELENGTHS

<u>CHANNEL</u>	<u>RADIANCE</u>	<u>WAVELENGTH BAND</u>
1	visible	0.58 - 0.68 μm
2	red visible; near infrared	0.70 - 1.10 μm
3	near infrared	3.50 - 3.90 μm
4	thermal infrared	10.3 - 11.5 μm
5	thermal infrared	11.3 - 12.4 μm

indication of surface and cloud-top temperatures. Only lower atmospheric features, specifically stratocumulus clouds and suspended aerosols, were considered in this thesis as upper and mid-level cloud areas were removed from the data set. Therefore, the radiative effects of such mid-level and upper-level atmospheric elements will not be discussed.

1. Channel 1

AVHRR channel 1 detects radiant energy in the relatively short wavelength band centered at .63 μm , characterized by yellow to red visible light. The smallest elements in the atmosphere are gaseous molecules. Absorption by these molecules is by definition, minimal in the visible wavelength window. The wavelength to element size relationship dictates that Rayleigh scattering will occur at each photon-molecule interaction.

Suspended aerosols such as dust particles, smoke, pollutants and sea salt are much larger than the gaseous molecules, and the scattering pattern for these constituents approaches the Mie solution. The scattering effects on the radiant energy detected by channel 1 are a function of wavelength, particle size distribution and aerosol composition. The size of these aerosols is highly variable, but their size distribution can generally be characterized as maritime or continental in origin (Shettle and Fenn, 1979). Maritime aerosols are primarily sea salt particles released into the lower atmosphere by wind wave action over oceanic waters. Their size distribution is significantly weighted toward particles with radii greater than 1 μm . Conversely, the size distribution of continental aerosols is weighted toward particles with radii generally less than 1 μm . These continental particles are deposited in the atmosphere by surface wind action, refinery burn-off or exhaust, and fires, usually in much greater number than marine aerosols. Measured reflectance from these continental aerosols should be higher due to the presence of more particles and, in part, the relative size of these particles (smaller particles are less forward-scattering from the Mie solution). Surface reflectance in this visible wavelength band is minimal, and relatively uniform over the ocean. Aerosol reflectance and its variations will dominate the reflectance characteristics received over cloud-free regions (Fett and Isaacs, 1979).

Stratocumulus cloud reflectances in channel 1 represent the effects of several cloud properties, although some of these properties are more important scattering factors than others in this wavelength band. The single scattering albedo (ω_0), representing the percentage of incident radiance that will undergo scattering in a single

scattering event (Liou, 1980), is approximately 1.0 for liquid water in this visible wavelength band (Hunt, 1973). This implies that each photon interaction with a water droplet results in total scattering attenuation with no absorption. Thus, clouds composed of water droplets exhibit similar absorption and scattering characteristics to those water droplets. However, the complexity of the cloud structure presents other factors which influence the cloud reflectance properties. The cloud characteristics that affect reflectance at visible wavelengths are the cloud liquid water content, cloud thickness, the particle size distribution and composition, cloud shape and sun-cloud-satellite geometry.

Although, stratocumulus clouds are layered, which creates a uniform high reflectance relative to clouds of finite size, the structure of individual elements of stratocumulus contribute to variations in the reflectance. Also, the liquid water content, particle size distribution, and particle composition influence cloud reflectance properties. Suspended aerosols contribute the cloud condensation nuclei (CCN) on which water collects to form cloud droplets. CCN composition and size determine the initial rate of water droplet growth. Nieburger *et al.* (1971) described the influence of these two factors. Some particles are strongly hygroscopic like sea salt and absorb water readily, even at humidities less than 100 percent. The composition of other particles may be hydrophobic and resist condensation, retarding droplet formation. In addition, as these CCN become larger, droplets form more readily on their surfaces. For example, nuclei greater than 1 μm radius require only 0.1 percent supersaturation for condensation, while the same type of particle with only a 0.6 μm radius requires a 0.2 percent supersaturation for droplet formation. Thus, the particle size distribution has a direct impact on the cloud droplet sizes and size distribution. Once a droplet has formed around the CCN, the size distribution and available liquid water become more influential on the droplet growth and its reflectance.

The size of the cloud droplets is also dependent upon the liquid water content, where more water allows for larger and a greater number of droplets to develop. Since water collects on suspended particles in the atmosphere, the resultant cloud water droplets are significantly larger than the CCN. The scattering pattern becomes subject to ray optic principles at visible wavelengths. Therefore, larger cloud water droplets are more reflective than the smaller cloud droplets. Hence, a higher liquid water content generally infers greater reflectance since more water is present in the form of droplets.

Cloud thickness affects the number of interactions between photons and water droplets. An increase in initial and multiple scattering events occur in thicker clouds, which results in greater cloud reflectance. Although all of the described cloud characteristics determine the reflectance detected by channel 1, the liquid water content and stratus thickness have the greatest influence. However, the cloud droplet number and size distribution may have a greater effect on the cloud reflectance at other wavelengths, specifically 3.7 μm as in channel 3 of the AVHRR.

2. Channel 2

The red visible to near infrared radiance wavelengths detected by channel 2 are just slightly longer than the visible wavelengths detected by channel 1, and the reflectance characteristics of the surface, stratocumulus clouds, suspended aerosols and gaseous molecules are very similar for each channel. As noted previously, reflectance generally decreases as the scattering element size decreases with a constant wavelength. The argument follows that the reflectance will also decrease as the wavelength increases if the scattering element remains the same size. Rayleigh scattering, typified by gaseous molecules at these wavelengths, is proportional to the inverse fourth power of the wavelength ($\propto \lambda^{-4}$) and therefore 70 percent less reflectance is expected in channel 2. Suspended aerosols again produce Mie scattering of the incident radiance at channel 2 wavelengths, and these features will dominate the reflectance values in cloud-free regions as they do in channel 1. The same conclusions about minimal and uniform surface reflectance in channel 1 can be applied to channel 2. Stratus clouds will also produce lower reflectances at the red visible to near infrared wavelengths, representative of similar cloud characteristics as those observed at the shorter visible wavelengths.

3. Channel 3

The radiant energy detected in the near infrared window with AVHRR channel 3 consists of backscattered solar radiation and emitted radiation from clouds and the surface. The emitted radiance is separated from the total radiance using channel 4 measurements (discussed in the following section) through the Planck function. This process is discussed in more detail in the Chapter III. Measurements in the near infrared window were evaluated only in the case of stratocumulus clouds. Hence, the reflectance, scattering and absorption characteristics of other features like suspended aerosols and the surface are not discussed. Gaseous absorption will again be minimal in this atmospheric window with only slight water vapor absorption (Fig.

2.1). The gaseous molecules will produce Rayleigh scattering, but the wavelength dependence of this scattering solution ($\propto \lambda^{-4}$) greatly decreases their effect.

The single scattering albedo for stratocumulus clouds in this wavelength band is approximately 0.75 (Hunt, 1973), which implies that a 25 percent chance of absorption and a 75 percent chance of scattering exists for each single interaction between a photon and a cloud water droplet. Essentially all of the incoming electromagnetic energy at this wavelength is absorbed by stratocumulus clouds that are at least fifty meters thick due to sufficient multiple scatters and ultimate absorption.

The reflectance properties of these clouds is less dependent on the cloud thickness and liquid water content than at visible wavelengths. As Hunt (1973) noted, the droplet size distribution is the major reflectance modifier. The water droplet sizes approach the magnitude of infrared wavelengths, which results primarily in Mie scattering. According to Mie theory, larger cloud droplets are more forward-scattering than smaller cloud droplets. Thus, greater reflectance is associated with smaller cloud droplets. The size of these droplets correlates to their CCN origin. Sea salt tends to form large water droplets since the particles are initially larger and water collects on them rapidly. Particles of continental origin are generally smaller and may be more resistant than sea salt to water collection due to their chemical nature. Cloud water droplet growth can be further restricted by continental CCN since these aerosols occur in greater number than marine CCN. As a result, stratocumulus clouds of continental CCN origin are often composed of many smaller water droplets, whereas clouds of marine CCN origin contain relatively fewer, but larger, water droplets with the same liquid water content. Twomey (1977), in studying the effects of pollution on cloud reflectances which can be correlated to continental-like CCN effects, noted that a droplet concentration increase corresponds to a cloud optical thickness increase, thereby also increasing the cloud reflectance. Although this also increases the radiant absorption in the cloud (which decreases the reflectance), Twomey's calculations indicated that the former process was dominant. From these arguments, the satellite will detect greater reflectance from the continental-type clouds than from the marine-type clouds.

4. Channel 4

Atmospheric gases, suspended aerosols, clouds, and the ocean surface are in a temperature range that produces maximum emissions in the channel 4 wavelength band. Thus, satellite measurements with channel 4 can detect this emittance, which

can then be converted to a temperature, hence the term 'thermal' infrared to describe this wavelength. The infrared radiation emitted from the ocean surface represents a 'skin' temperature because the photons are emitted from only the upper 0.05 mm of the water column. Additionally, evaporation at the ocean surface creates at least a thin layer of saturated water vapor in this region. Some minor absorption by water vapor occurs in this channel window, so a little absorption of sea surface emittance takes place. Therefore, the sea-surface temperature detected via the AVHRR is cooler than the observed temperature due this water vapor absorption.

Reflectance of solar radiation by the ocean surface is negligible since most of the incoming radiance is absorbed. Gaseous molecules and suspended aerosols are extremely small relative to the infrared wavelength, which produces Rayleigh scattering. Therefore, reflectance by molecular constituents is small and can be neglected at infrared wavelengths due to the wavelength dependence of Rayleigh scattering ($\propto \lambda^{-4}$).

The single scattering albedo for stratocumulus clouds in the thermal infrared wavelength band is approximately 0.45 (Hunt, 1973), which infers that greater than 50 percent chance of absorption occurs each time a photon interacts with a cloud water droplet. Infrared solar radiation is totally absorbed within about the upper ten meters of the cloud due to sufficient multiple scatters and ultimate absorption. Reflectance of solar radiation will be small since most of the incoming radiance is absorbed. The clouds also emit radiant energy at this wavelength back into the atmosphere. Thus, the satellite will detect emitted radiation from cloud tops that can be converted to temperatures in order to provide height information on these cloud tops.

C. MULTI-SPECTRAL RELATIONSHIPS

Additional information about the earth's surface and atmosphere can be acquired through channel ratios to highlight the wavelength dependence of scattering and absorption. The visible and near infrared wavelength ratios of channel 1 to channel 2 over cloud-free regions are very sensitive to the particle size distributions of suspended aerosols (Durkee, 1987). However, these same channel ratios with stratus cloud reflectances are not responsive to a specific cloud characteristic, but are indicative of a combination of cloud properties. An application of the channel 1 to channel 3 ratios for stratus cloud reflectance is to highlight the variations of the droplet number and size distributions of stratus cloud.

1. Channel 1/Channel 2 Ratio

As noted previously, suspended aerosols scatter visible solar radiation according to the Mie scattering solution. Surface reflectance is minimal in each wavelength band of channel 1 and channel 2 so that the aerosol effects dominate the reflectance values in cloud-free regions. Reflectance is thus heavily dependent upon the particle size distribution of these aerosols. The particle reflectance detected by channel 1 is generally greater than that detected by channel 2 since longer wavelengths experience increased forward-scattering in Mie theory. The ratio of channel 1 to channel 2 reflectance enhances the variations between aerosol size distributions in the cloud-free atmosphere. A size distribution with more small particles will display a significantly greater difference between the Channel 1 and Channel 2 reflectance than a size distribution weighted toward more large particles. Thus, the reflectance ratios for continental aerosols with high numbers of smaller particles will be greater than the ratios for marine aerosols with relatively larger particles (Durkee, 1987).

The scattering pattern of the much larger water droplets in clouds is subject to ray optics criteria at the visible wavelengths of channel 1 and channel 2. The complexity of geometric scattering and stratocumulus cloud structure makes the interpretation of the reflectance ratio extremely complicated. The resulting pattern may reveal some potential information about the reflectance, absorption and transmission relationship of the cloud, or possibly even the amount of cloud in a small area (pixel). Over a larger area this could imply the existence of individual cloud elements or a layer of stratus.

2. Channel 1/Channel 3 Ratio

At the near infrared wavelengths detected by channel 3, the scattering pattern of cloud water droplets is in accordance with the Mie scattering solution (recall that emittance has been subtracted from the total radiance at channel 3). Therefore, a lower ratio of the channel 1 to channel 3 reflectance is expected from clouds with a continental-type CCN size distribution, which would form a cloud water droplet size distribution with generally smaller droplets. Greater reflectances are detected from stratus with a more droplets and size distributions weighted toward smaller droplets like those formed from continental CCN sources. In the visible wavelength band of channel 1, greater reflectance is detected from the thicker clouds with higher liquid water content. Thus, the ratio would also become smaller from the detection of thin clouds with a low liquid water content, causing less channel 1 reflectance.

Additionally, a positive correlation tends to exist between these cloud characteristics. Stratocumulus clouds formed from continental CCN are often relatively dry and thin compared to the thick moist clouds formed over the ocean with marine CCN.

Conversely, a high channel 1 to channel 3 ratio is expected from stratocumulus clouds with larger water droplets formed from the particle size distribution of larger sea salt particles. The ratio becomes greater since the channel 3 reflectance is decreased relative to the smaller continental-type cloud droplets. Thick clouds with a higher liquid water content will relatively increase the visible reflectance of channel 1, and therefore the ratio. Again, a positive correlation generally exists between these features.

III. DATA ANALYSIS

A. DATA DESCRIPTION

The data set consists of images received from the NOAA-9 satellite, which is a member of the TIROS-N family of satellite systems. It uses a sun-synchronous low polar-orbit, so that coverage of the same geographic areas is provided at the same approximate sun-time each day. Back-scattered and emitted radiation is detected by the AVHRR system aboard this satellite. As stated previously, this cross-track scanning instrument receives radiation in five absorption windows of the electromagnetic spectrum. Designated as channels, the bandwidths of these windows are listed in Table 1. The five-channel AVHRR has a ground resolution of approximately 1.1 km by 1.1 km at nadir, degrading to 1.1 km by 4.25 km at the edges of the image. Data collection was performed at the Scripps Institution of Oceanography in La Jolla, California on magnetic tape.

The NOAA-9 satellite was in an ascending node, crossing the equator from south to north, as the daytime data passes were collected. Areal coverage is over the eastern North Pacific Ocean and the western portion of the North American continent. The summary consists of afternoon images in the late summer of 1986. Dates include the first two days of September and sixteen days in August; the 1st - 5th, 10th - 14th, 21st - 23rd and 29th - 31st.

The meteorological conditions on these dates were remarkably consistent with the climatology for that time of year. The National Weather Service upper level and surface analyses were closely examined for each date. At the 500 mb level, a blocking ridge centered roughly over the far western United States persisted throughout the time period. The strong 500 mb polar jet remained well north of the western United States coastline and eastern North Pacific Ocean, steering all migrating short waves to the northeast and over the high pressure ridge.

The dominant surface feature for this period was the eastern North Pacific Ocean subtropical high pressure system, usually centered near 40°N 135°W and fluctuating between 1024 mb and 1036 mb. This center pressure variation influenced the pressure gradient strength along the coastline, thereby modifying wind velocities. The anti-cyclonic circulation creates mostly northerly surface flow over and along the coast,

although the land sea breeze effect dominates this flow with a generally weak pressure gradient. Two very weak slow-moving cold fronts approached the area from the northwest, but stalled and dissipated before intruding into it. Hurricane Javier quickly transited westward along the 20°N latitude late in August, but it had been downgraded to a tropical storm during the data period and it did not affect the analyzed region.

Due to the typical meteorological pattern of these dates in 1986, it is concluded that a summary of the atmospheric data, specifically stratocumulus cloud information, over this area would be climatologically significant and accurate. There were no anomalies such as storms or weather fronts to inject special considerations into the data set.

B. DATA PROCESSING

The analysis area extends from 25°N latitude to 50°N latitude, and ranges longitudinally from 115°W to 140°W. The region is depicted in Fig. 3.1. It was divided into boxes of 0.1° by 0.1° dimension. This size equates to approximately 100 pixels per box, roughly 10 pixels by 10 pixels or 10 km by 10 km. Therefore, a square grid of 251 by 251 boxes covered the area.

From the digitized data provided on tape, radiance values for each pixel were calculated at all four channels. This satellite-measured radiance (L), both emitted and backscattered, is approximated by Eqn. 3.1.

$$L = \epsilon B(T) + r(\theta_0, \theta, \phi) I \cos \theta_0 \quad (3.1)$$

The first term on the right hand side represents the thermal emittance. $B(T)$ is the blackbody intensity as a function of temperature and ϵ is the emissivity, defined as the ratio of the actual emitted radiance of a medium to a perfect blackbody's emitted radiance. Thus, the emissivity of a blackbody is equal to 1.0. Kirchoff's law states that the absorptivity of a medium is equal to its emissivity.

The second term on the right hand side of Eqn. 3.1 represents the backscattered solar radiation. The incident solar radiation (I) is modified by the cosine of the solar zenith angle (θ_0), which normalizes this radiance to a 0° solar zenith angle. The reflectance of the medium is characterized by $r(\theta_0, \theta, \phi)$, which is a function of the solar zenith angle (θ_0), satellite zenith angle (θ), and relative azimuth (ϕ) as depicted in the sun-earth-satellite geometry of Fig. 3.2.

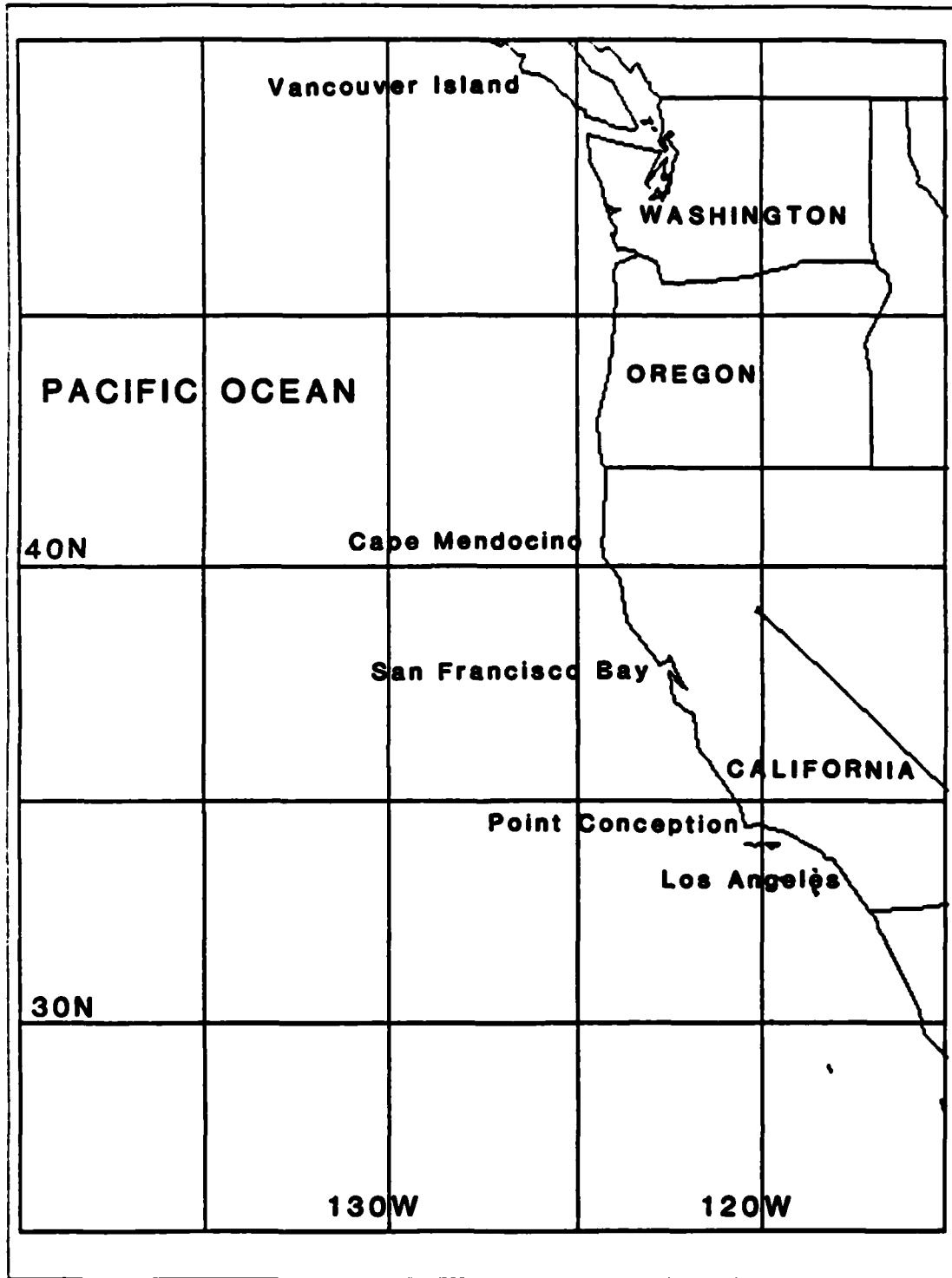


Fig. 3.1 Summary area.

The radiances detected by AVHRR channel 1 and channel 2 are strictly backscattered solar radiances with no emittance. Both of these channel values are measured bidirectional reflectances, calibrated in terms of albedo (Lauritson *et al.*, 1979).

AVHRR channel 4, on the other hand, detects only thermal emittance from the surface and atmospheric elements. This emittance is converted to a temperature through the Planck function, Eqn. 3.2.

$$B_{\lambda}(T_{\lambda}) = \frac{2hc^2}{\lambda^5(e^{hc/K\lambda T} - 1)} \quad (3.2)$$

This wavelength-dependent blackbody intensity is a function of the absolute temperature (T). Other terms include Planck's constant (h), Boltzman's constant (K) and the speed of light (c). A non-linearity correction factor is applied through an interpolation polynomial (Gerald and Wheatley, 1984) with temperature corrections from the NOAA calibration manual (Lauritson *et al.*, 1979). Thus, a temperature is derived from the thermal infrared emittance detected by channel 4.

AVHRR channel 3 includes both thermally emitted radiance and backscattered solar radiance. However, only the reflectance is desired from the detected irradiance. Allen (1987) used a unique process that utilized the channel 4 radiance measurements to separate the near infrared backscattered solar radiance from the thermally emitted radiance in channel 3. This same method was applied in this thesis to isolate the cloud reflectances in Channel 3. First, two major assumptions were made in this procedure (Ruff and Gruber, 1983). Atmospheric attenuation by features other than clouds was assumed to be negligible. This is a reasonable assumption since channel 3 is in the atmospheric absorption window (Fig. 2.1) and the wavelength-dependent Rayleigh scattering ($\propto \lambda^{-4}$) of these molecular atmospheric elements at this wavelength is small. Cloud emissivity was assumed to be 1.0 so that thermal emissions in channel 3 could be derived directly from channel 4 emittance measurements. Allen (1987) remarked that the reflected solar radiance is considerably larger than the cloud thermal emittance, and this implies that the liquid cloud measurements should contain a very small resultant error in the emittance value from this emissivity assumption relative to other surfaces.

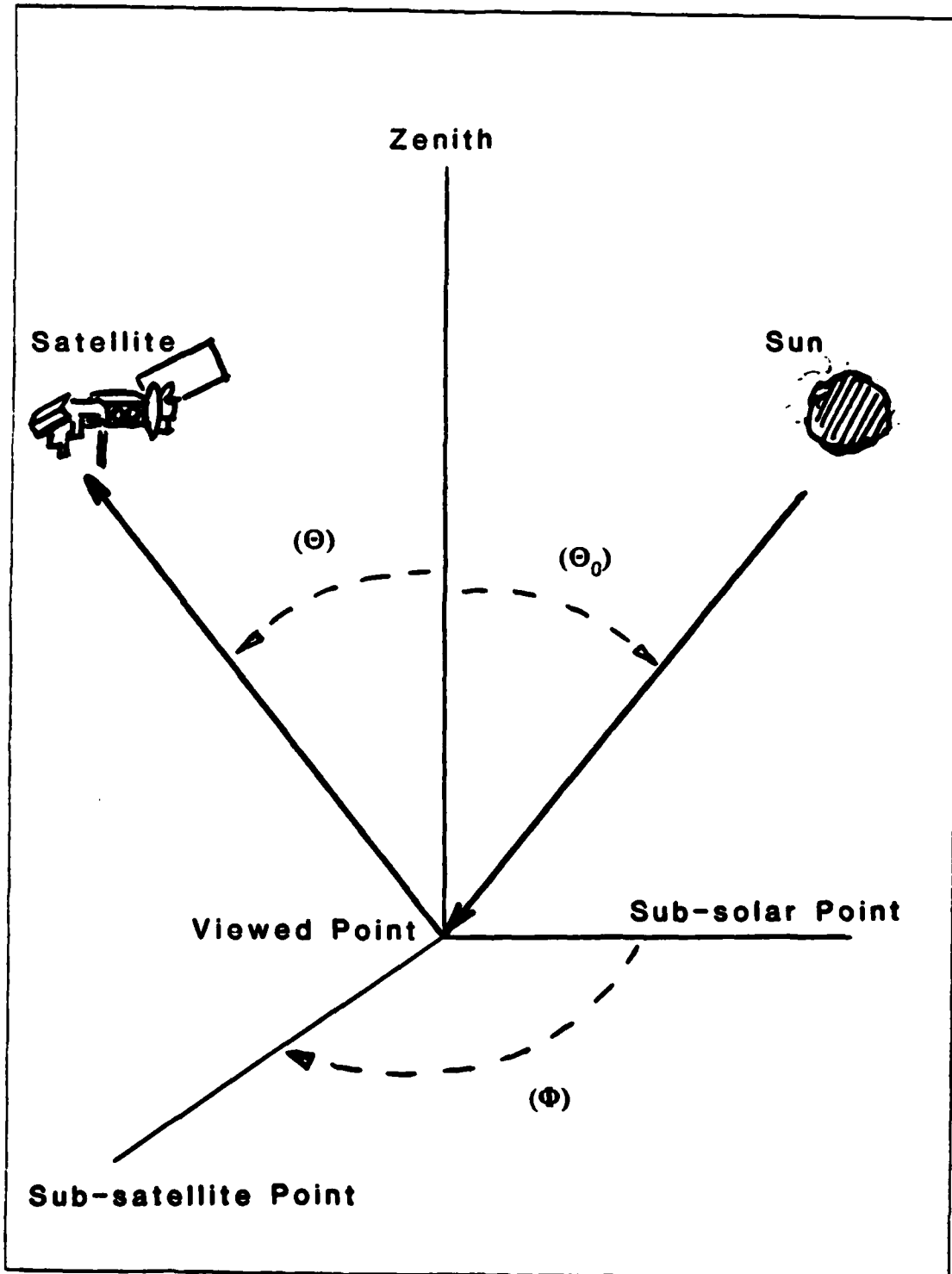


Fig. 3.2 Sun-earth-satellite geometry.

The channel 3 emittance is estimated from the channel 4 radiance through the wavelength-dependent Planck function, Eqn. 3.2. This emitted radiance is then subtracted from the total radiance detected by channel 3, providing desired backscattered solar radiation. The channel 3 value is determined by solving Eqn. 3.1 for the reflectance, given by Eqn. 3.3.

$$r_3 = \frac{L_3 - B_3(T)}{(I_3 \cos \theta_0) f - B_3(T)} \quad (3.3)$$

The additional variable (f) is the anisotropic reflectance factor (ARF). Most scattering as revealed in the preceding chapter is not isotropic so that the sun-satellite geometry (Fig. 3.2) has a significant effect on the detected reflectance. In order to distinguish and compare these reflectances based on theoretical assumptions, all of the pixels must be viewed from the same perspective. Taylor and Stowe (1984) developed an atlas of anisotropic reflectance factors (ARF) to apply to these pixel values as a geometric correction. The ARF is defined by Taylor and Stowe (1984) as "a ratio between radiance in a given direction and the radiance that would result if the surface reflected isotropically". It is a function of surface type, solar zenith angle, satellite zenith angle and relative azimuth, and was determined from satellite measurements and calculations.

The ARF is applied only to detected cloud cases with reflectance (channels 1,2, and 3) using the 'low cloud' surface type data in the atlas. The factors are set up in a matrix as a function of solar zenith angle range and bin number. These bins are determined by a range of satellite zenith angles and relative azimuths. The correct ARF is thus selected for each pixel based on these factors, and then multiplied by that pixel value to achieve a geometrically-adjusted reflectance.

The processing of the satellite data was performed on a Digital VAX/VMS cluster that included a VAX 8250 and three MicroVAX II's in the new Meteorology/Oceanography Interactive Digital Environmental Analysis Laboratory (IDEA Lab) at the Naval Postgraduate School. The first procedure was navigation of the satellite passes through a manual interface point-positioning system. Because the images were produced from daytime passes, contamination due to sunglint had to be removed from the data. Potential thresholds were considered to detect areas of sunglint and then remove the contaminated pixels, but a conservative method was

utilized instead to ensure complete elimination of the sunglint-affected pixels. Since these were afternoon passes, the sun-satellite geometry produced sunglint in the western portion of the image. Therefore, this half of each image was deleted from the data set.

The next procedure was to classify the pixel as cloud or cloud-free. Two thresholds were established from manual pixel value evaluation of several satellite images in the data set. This process involved visual identification of the ocean surface and different clouds in channel 2 and channel 4. Then the pixel values in these channels were examined at clear points, cloud points and cloud edge points. A pixel was determined to be cloud-free if two conditions were satisfied:

- (1) the channel 2 reflectance was less than or equal to 0.153.
- (2) the channel 4 temperature was greater than or equal to 271.1.

If the pixel was classified as cloud-free, then the channel 1 and channel 2 reflectances, channel 4 temperature and channel 1/channel 2 ratio were computed. If the pixel was determined to contain cloud as a result of exceeding the cloud-free thresholds, another threshold test was run to establish whether it was a low stratocumulus cloud or not. A process similar to the preceding one was used to set up the new thresholds. A pixel was classified as stratocumulus cloud if the two following conditions are met:

- (1) the pixel was not classified as cloud-free from the previous threshold test.
- (2) the channel 4 temperature was greater than 271.1 (to eliminate higher clouds).

The computations for these stratus cloud pixels included channel 1, channel 2 and channel 3 reflectances, channel 4 temperature, and channel 1/channel 2 and channel 1/channel 3 ratios. It is again noted that the ARF was applied to the reflectances of low cloud-classified pixels in channels 1, 2 and 3.

The classification scheme was examined and confirmed that the thresholding process achieved the desired results separating cloud and cloud-free regions, and stratocumulus from mid-level and upper-level clouds. Once the pixel was classified and the various channel and ratio calculations were completed, the values were added to the appropriate box on the grid. A cloud-free and stratocumulus cloud pixel count was also conducted for each box. After all eighteen passes were processed, a separate program accepted this file to calculate an average and a standard deviation for the cloud-free and stratocumulus cloud computations for each box. These results were

scaled so that they could be displayed in image format, and the results are discussed in the following chapter.

IV. RESULTS

The results of the satellite radiance climatology are displayed and discussed in the following sections of this chapter. First, the cloud-free cases are examined, starting with the cloud-free pixel summations. The amount of data in an area derived from these counts must be considered in analyzing the average values and standard deviations of each channel and each spectral ratio. The other cloud-free cases, in order of discussion, include the channel 1 reflectances, the channel 1:channel 2 reflectance ratios with a brief examination of the channel 2 reflectances and the channel 4 temperatures. Maximums and minimums will be highlighted within the analysis area in each case with explanations for their occurrence. The reflectance and reflectance ratio analyses will concentrate on suspended aerosol effects, while the channel 4 temperature analysis will be representative of the surface temperature field.

Next, the stratocumulus cloud cases will be discussed. Again, the pixel summations are examined first, followed by an analysis of the average values and standard deviations for each channel or channel ratio. These consist of the channel 1 reflectances, the channel 1:channel 2 reflectance ratios with a short discussion of the channel 2 reflectances, the channel 3 reflectance residuals (thermal radiance is removed from the total radiance at this wavelength), the channel 1:channel 3 reflectance ratios and the channel 4 temperatures. Each of the cases will emphasize those cloud characteristics which have the greatest effect on the radiance and its variation.

A. CLOUD-FREE CASES

1. Pixel Counts

The cloud-free pixel summations are displayed in Fig. 4.1. Large pixel counts indicate mostly cloud-free regions, but low pixel counts do not necessarily imply cloudy areas. Such low pixel counts may also result from a lack of data. This is most applicable in the western portion of the analyzed area as evidenced by the zero-valued southwestern corner of the cloud-free pixel count image, and clearly seen in subsequent data images. Since each of the eighteen satellite passes covered a slightly different area, 'striping' of western data can be seen from the northwest to the southeast due to lack of overlapping images in the region. The data decrease toward this edge is due to the geographic receiving limitation of the HRPT location in La Jolla, California. This



Fig. 4.1 Cloud-free pixel counts.

is reduced further when the data editing for sunglint is incorporated since this procedure removes the entire western half of the satellite pass.

The major feature of the cloud-free pixel count image (Fig. 4.1) is the maximum area, greater than 1200 pixels, on the coast of northern California just north of Cape Mendocino. The mostly cloud-free region expands from this clear center in all seaward directions, notably offshore and to the southwest. This is in contrast with the climatological norm, which usually finds this area covered by a layer of low stratus. However, Dorman (1987) hypothesized that major wind reversals along the northern California coast can occur during the summer, which also create a boundary to the stratus with significant clearing to the north. Southerly winds will develop along this portion of the coast, although the analysis of coastal stations will often miss them. Dorman's theory is that gravity currents or Kelvin waves in the marine layer form in the Southern California Bight, and then progress northward until a blocking wave interrupts them. An eddy thus forms in this spot, and the disturbance reverses the typical northerly surface wind flow. These wind reversals with the resultant clearing will often last for periods consisting of a few days, as has apparently occurred during the analysis period.

A thin line of clearing extends along the coastline from Point Conception past San Diego with a clearing maximum of at least 1100 cloud-free pixels centered near Los Angeles. This feature is climatologically significant and typical for the Southern California Bight in late summer. Lee *et al.* (1980) presented several explanations for this clearing pattern linked to the synoptic-scale flow, topography, sea surface temperatures (SST) and land/sea breezes. Synoptically, moist marine air flow along the central California coast continues past Point Conception without turning into the Southern California Bight. The flow is thus offshore across the northern coast of the bight, and the clearing represents dry air that flows off the continent from inland valleys. Topographically, the Arguello headland north of the Santa Barbara Channel extends west to east with coastal heights up to 700 meters. This land mass acts as a wall to the northerly to northwesterly flow around the synoptic-scale Pacific high circulation, creating convergence and orographic lifting as well as a low stratus boundary. Downwind divergence lowers the inversion base and causes subsidence warming on the leeward side of the headland. Both processes enhance the small area of clearing in the coastal stratus at this spot. This effect is also seen near islands. San Clemente Island created a persistent clear area just downwind (south) from its position and is evident in Fig. 4.1.

Warm SST in the Southern California Bight, especially near the coast, as evidenced in the cloud-free thermal infrared data image of Fig. 4.5a (discussed later in this chapter) may heat the marine layer so that additional daytime warming from above can evaporate the cloud droplets. The increasing clearing to the south is a consequence of these processes with additional solar heating and even warmer SST. The daytime sea breeze along the southern California coast carries the marine layer air over the warm water, but the breeze weakens at night and the lack of solar heating allows the stratus to reform. Of course, these data include only daytime afternoon passes when heating factors are most influential.

The sea land breeze plays a more significant role in coastal stratus dissipation over southern California than over regions to the north. This is partly due to the more intense daytime heating and large open basin of Los Angeles which presents ideal conditions for development of the sea breeze circulation. Offshore subsidence corresponds to this sea breeze, and dissipation of stratus cloud over water increases seaward throughout the day (Lee *et al.*, 1980). The data set includes only afternoon (approximately 2130 to 2300 UT, or 1430 to 1600 local) images when the sea breeze effects are maximized, and the pattern of cloud-free pixels reflect this.

2. Channel 1 Reflectances

The channel 1 reflectance averages for cloud-free conditions are depicted in Fig. 4.2a with the standard deviation presented in Fig. 4.2b. Extremely large reflectance averages, greater than 0.17, are found in the northwest corner of the analyzed area and just south of Point Conception, extending southwestward in a band to the corner of the area. These regions correlate very closely to the data minimums in Fig. 4.1. The magnitude of these averages indicates that some partial cloud may be present in the pixels since the values are much greater than would be expected from the sea surface or suspended aerosols. This argument for potential contamination of cloud-free classified pixels is enhanced by the determining thresholds, which were established to ensure accuracy in the stratocumulus cloud detection and minimize contamination of the stratus cloud cases. The anomalous results in the channel 1, channel 2 reflectance ratios and channel 4 temperatures over these same locations (discussed in later sections) add further support to the conclusion of partial cloud contamination in the cloud-free cases.

Relative reflectance maximums at 0.10 to greater than 0.15 are present in the Southern California Bight, while generally lower reflectances at less than 0.07 are



Fig. 4.2a Cloud-free channel 1 reflectances.

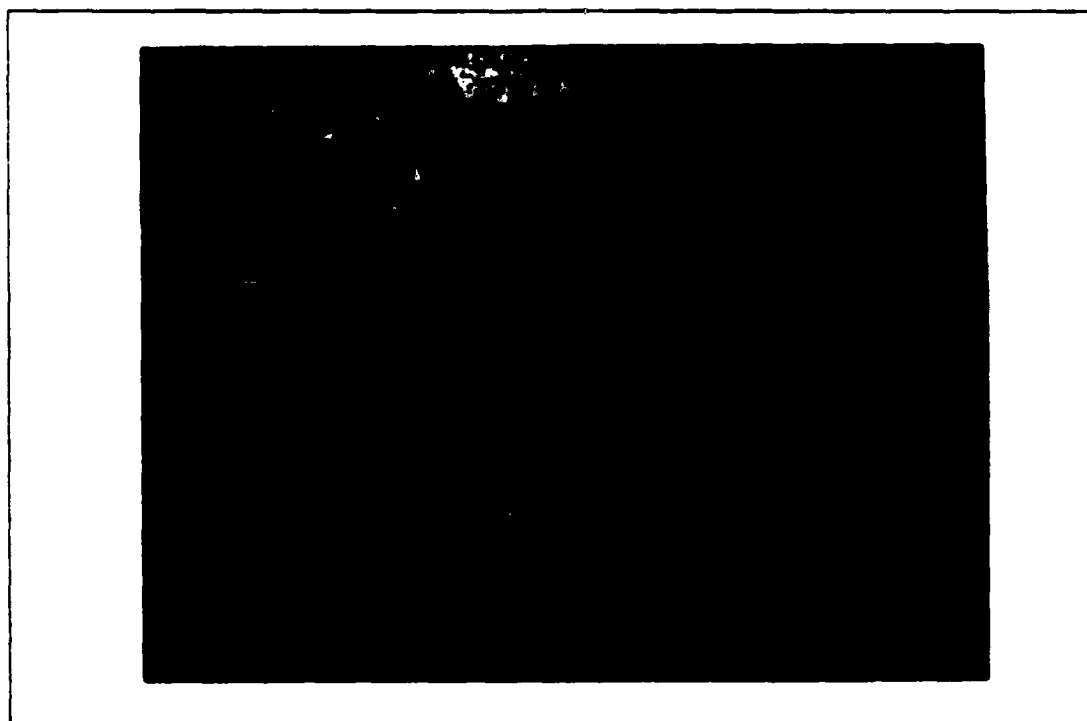


Fig. 4.2b Cloud-free channel 1 standard deviations.

located offshore from central California. The maximums may represent aerosol influences on the reflectance, specifically from a greater density of aerosols. The source of these particles may be continental. This would be expected in the Southern California Bight with the northerly offshore flow to transport continental particles over this area along with any pollutants from the populated and industrial Los Angeles basin. The maximum reflectance region in the northwest corner is too data deficient to determine any aerosol implications and may be contaminated by partial clouds as noted previously. The minimum areas represent maritime-like particle size distributions and or a lower aerosol density. Synoptic-scale flow into this region around the subtropical high is entirely over water to substantiate the presence of marine particulates.

An anomalously low reflectance center (~ 0.035) is located near $35^{\circ}\text{N } 130^{\circ}\text{W}$. The fact that it appears in a relatively data sparse area but with a minimum standard deviation indicates that this may not be a persistent phenomenon. This feature also appears in the measurements at other wavelengths, from which more conclusions will be drawn in subsequent sections.

The standard deviation of cloud-free channel 1 reflectances (Fig. 4.8b) provides information about the aerosol size and density variations and inferences of data coverage importance. Marine particle size distributions and their relatively small amounts tend to show greater variance in their respective reflectance properties as depicted over the northern ocean areas than the continental aerosols along the central California coast. The offshore ocean area shows a significant degree of variance, as does the coastal portion of the Southern California Bight, but this is probably due to the variability of the sea breeze which effects the amount of stratus burn-off each day away from the coastline. The northern and central California coastal regions have relatively small deviations, which imply persistent size distributions and aerosol numbers for continental particles in these locations.

The variance also may be driven by the possible contribution of partial clouds in the pixels. The smallest standard deviation (less than 5.0) corresponds directly with the suspected regions of cloud contamination extending southwestward from Point Conception and across the northern edge of the analysis area. As the variance increases, the potential cloud contamination would therefore decrease. The least contamination would occur over the other mid-ocean regions. However, the lower variances along the coast could be associated with lower pixel counts and not just potential cloud contamination.

3. Channel 1/Channel 2 Reflectance Ratios

Fig. 4.3a is the cloud-free channel 2 average reflectances and Fig. 4.3b is the corresponding standard deviations. These two figures correlate very closely to the channel 1 reflectance patterns represented by Fig. 4.2a and Fig. 4.2b, respectively. The patterns are nearly identical, as was theoretically expected, with the channel 2 reflectance values slightly lower than those of channel 1. Therefore, new information is not clearly revealed by these data images, but a comparison through the ratio of the two solar channels accentuates the reflectance differences. This can be seen in the channel 1 channel 2 reflectance ratio data image, Fig. 4.4a. The standard deviation of this ratio is depicted in Fig. 4.4b.

As discussed in Chapter II, this ratio is extremely sensitive to the particle sizes and their distribution. The entire continental coastline is bordered by high ratio values greater than 1.70, extending somewhat offshore with even greater ratio values off central California. These ratios infer continental-type particle size distributions, which are weighted toward smaller particles. Continental aerosols are expected along coastal regions as opposed to mid-ocean areas. An extremely high ratio outline with values ranging from 2.00 to greater than 2.13 extends south of the San Francisco Bay area, slightly past Point Conception. The standard deviation in Fig. 4.4b for this distinctive pattern is very small (less than 5.0) and matches the shape of the high ratio values. This would support the possibility that these ratios represent a single event plume of unique aerosols with a particle size distribution strongly weighted toward small particles. In theory these small particles are classified by radii less than 1 μm . Based on the surface synoptic situation, the aerosol source would be near the southern end of San Francisco Bay. One can speculate that these aerosols could be pollutants of some form, which are generally smaller and in greater number than typical continental particles.

Another area with a possible continental-like size distribution, implied from high ratio values (greater than 2.00), is the oceanic anomalous center identified previously by very low channel 1 reflectances. The low channel 1 reflectances in this spot are more representative of the small quantity of aerosols than the size distribution. Thus, a size distribution weighted toward small particles can be assumed. In correlation with the warm SST pool from Fig. 4.5a in the following section, it is hypothesized that these aerosols may be of oceanic origin. One possible source is sulfate particles suspended by the chemical reaction of DMS (di-methyl sulfate)

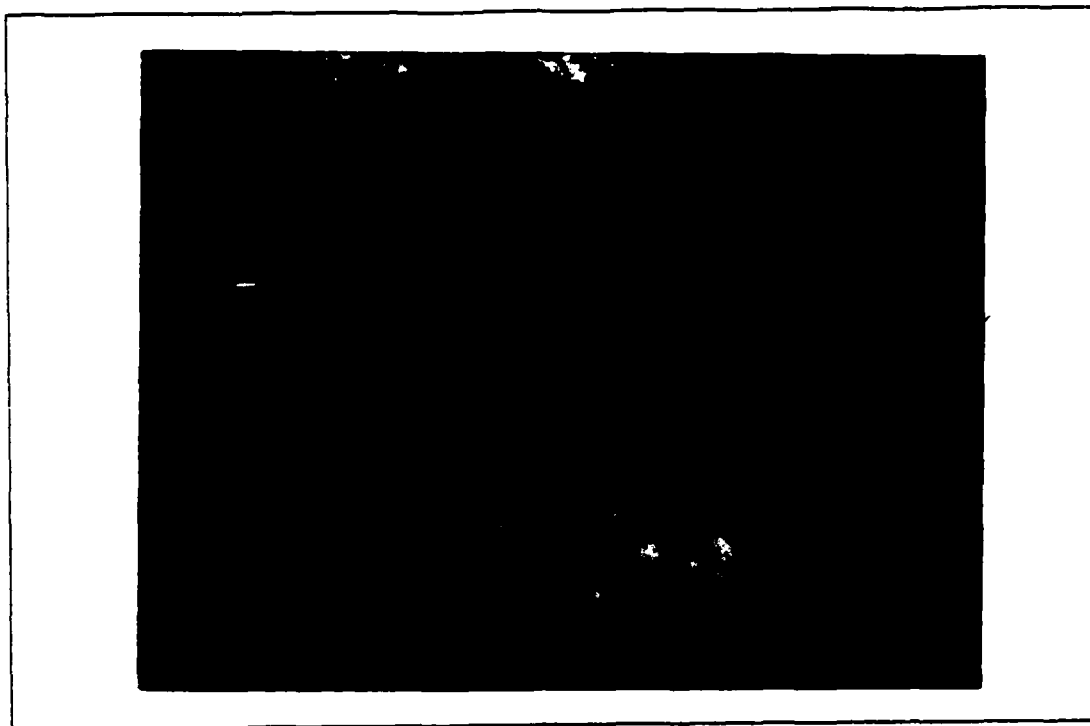


Fig. 4.3a Cloud-free channel 2 reflectances.

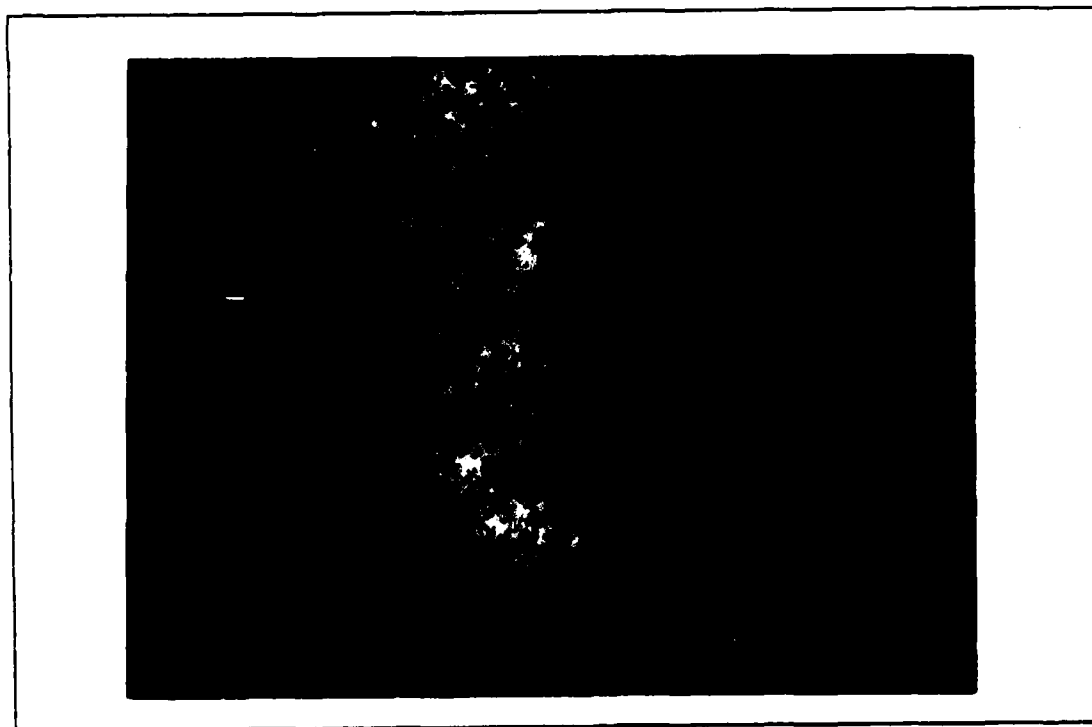


Fig. 4.3b Cloud-free channel 2 standard deviations.

released by phytoplankton near the surface (Charlson *et al.*, (1987). This implies that this distinct anomaly marks a concentrated region of planktonic activity or bloom.

The lower ratio values over the ocean areas represent aerosols with size distributions weighted toward large particles, most likely suspended sea salt. However, very low ratio regions extend southwesterly from Point Conception and exist in the northwestern corner of the analyzed area. These ratios, at less than 1.40, are small enough to suggest possible cloud contamination of the pixels. Correlation of this region with the zone of potentially contaminated pixels detected with the channel 1 reflectances supports this conclusion.

The standard deviation pattern mirrors those of the channel 1 and channel 2 reflectance variances. The ocean areas exhibit generally large standard deviations (approximately 23.0) except in the suspected contamination regions and along the data sparse western edge. The 'anomalous' area also shows little variance at less than 12.0. The largest values occur well offshore, implying highly variable particle size distributions amongst marine aerosols. Slightly smaller variances are located along the central California coastline, suggesting that these continental-like particle size distributions are relatively uniform.

4. Channel 4 Temperatures

The channel 4 radiances under cloud-free conditions represent surface emittances which can be converted to sea-surface temperatures. Fig. 4.5a depicts this average SST pattern with the standard deviations of these temperatures shown in Fig. 4.5b. Several significant features were revealed that agree closely with the climatological expectations of the area. The most striking of these is a pool of cold water with temperatures approximating 283.0 K to 285.5 K ($\sim 10.0^{\circ}\text{C}$ to 12.5°C), which provides evidence of a major upwelling event near Cape Mendocino, a common location for this phenomenon. Upwelling is a very typical summertime occurrence along the northern and central California coast. This results from the persistent synoptic-scale flow around the subtropical high that results in northerly surface winds along the coast. This induces offshore near-surface water transport, and very cold bottom water comes to the surface to replace the departed surface water. Cold water exists in a narrow coastal band from Vancouver Island to Point Conception in connection with the upwelling and the cold Davidson/California current. Also, two thin filaments of cold water at approximately 285.0 K can be detected extending westward about 25 km from the San Francisco Bay area.

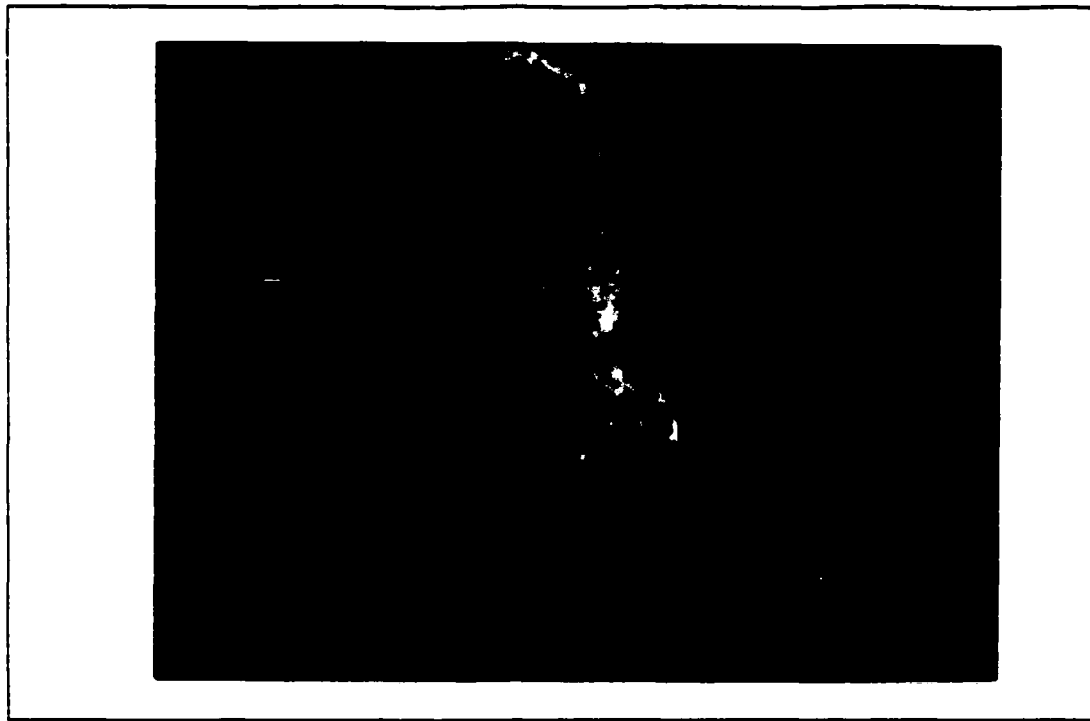


Fig. 4.4a Cloud-free channel 1/channel 2 reflectance ratios (x 100).

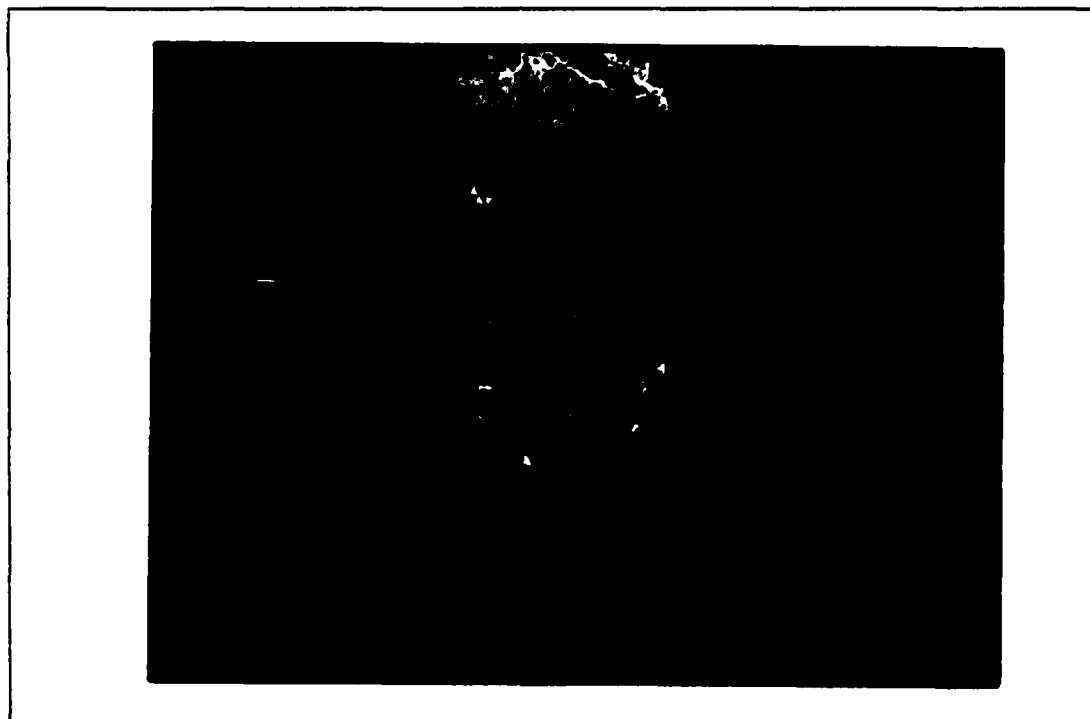


Fig. 4.4b Cloud-free channel 1/channel 2 ratio standard deviations.

A distinct zonal separation of SST exists approximately along the 45°N latitudinal. This feature possibly identifies the position of the subarctic oceanic front with colder surface water to the north and warmer surface water to the south. The relatively cold pool of water (less than 280.0 K) in the northwest corner of the analyzed area correlates to the region of suspected partial cloud contamination described previously since even low clouds are generally cooler than the sea surface. Also, the effect of potential cloud contamination decreases the calculated temperatures in the band extending southwestward from Point Conception.

The SST increases equatorward, especially in the Southern California Bight. Since this region is often clear as noted in the cloud-free pixel image (Fig. 4.1), solar radiation reaches all the way to the sea surface to heat it. This is also an area of relatively shallow shelf water, which enhances the warming process. Very warm surface water at greater than 291.0 K extends into the southern reaches west of Baja due to greater incoming solar radiation through the cloud-free atmosphere. The anomaly referred to earlier also appears in the SST data image as a pool of warm surface water with temperatures greater than 290.0 K.

Fig. 4.6 depicts the National Weather Service (NWS) monthly mean SST (actually a mean of twice-weekly analyses) for August 1986, determined from ship, bouy and satellite observations. The SST derived from thermal infrared radiance measurements (Fig. 4.5a) correspond closely to the monthly mean SST. For example, the coastal upwelling event north of Cape Mendocino and the extension of cold water southward along central California are well-defined and show remarkable correlation between the two analyses. The similarities are also demonstrated by the warm SST pattern in the Southern California Bight. However, the channel 4 temperatures are generally 1.5°C to 2.0°C (or Kelvin) cooler than the mean temperatures over the entire analysis area. The coldest SST in the upwelling region is approximately 10°C (~ 283 K) from the radiative measurements, but 12°C in the NWS analysis. The temperature difference is similar near Los Angeles, where the warm SST maximum is approximately 18.5°C (~ 291.5 K) according to channel 4 and 20°C in the mean. This small, but persistent, difference represents water vapor absorption of thermal infrared emittance in the saturated layer (from evaporation) just above the ocean surface. This absorption reduces the detected radiation by the AVHRR with channel 4, and thus cools the calculated SST relative to the observed SST.

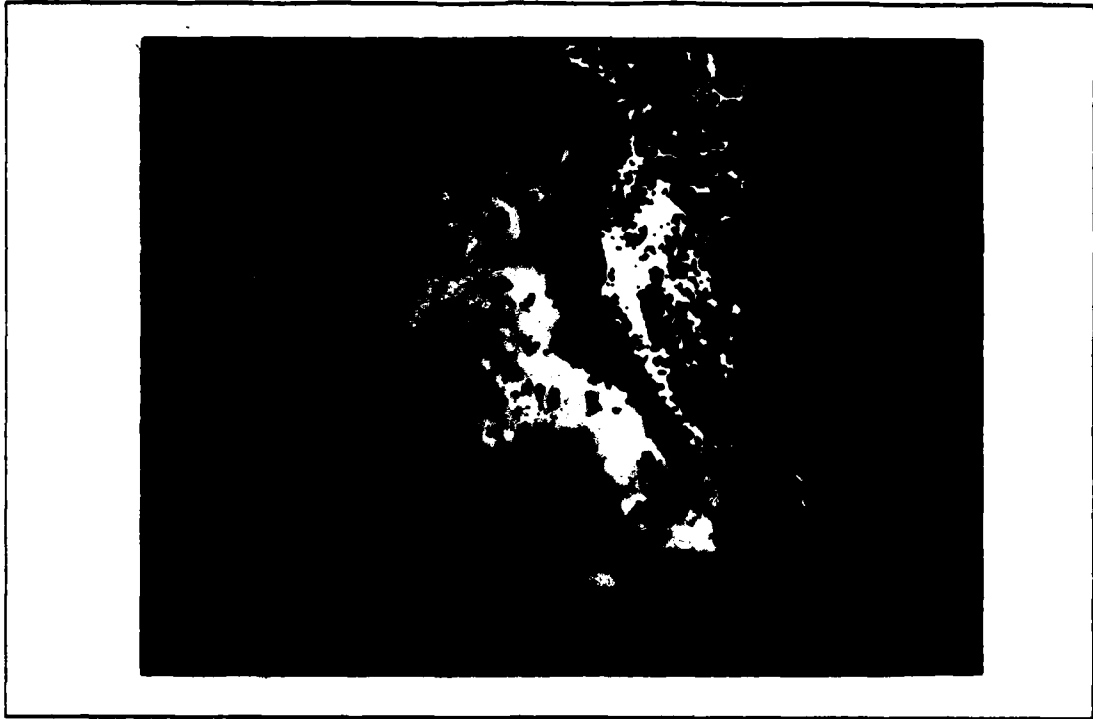


Fig. 4.5a Cloud-free channel 4 temperatures.

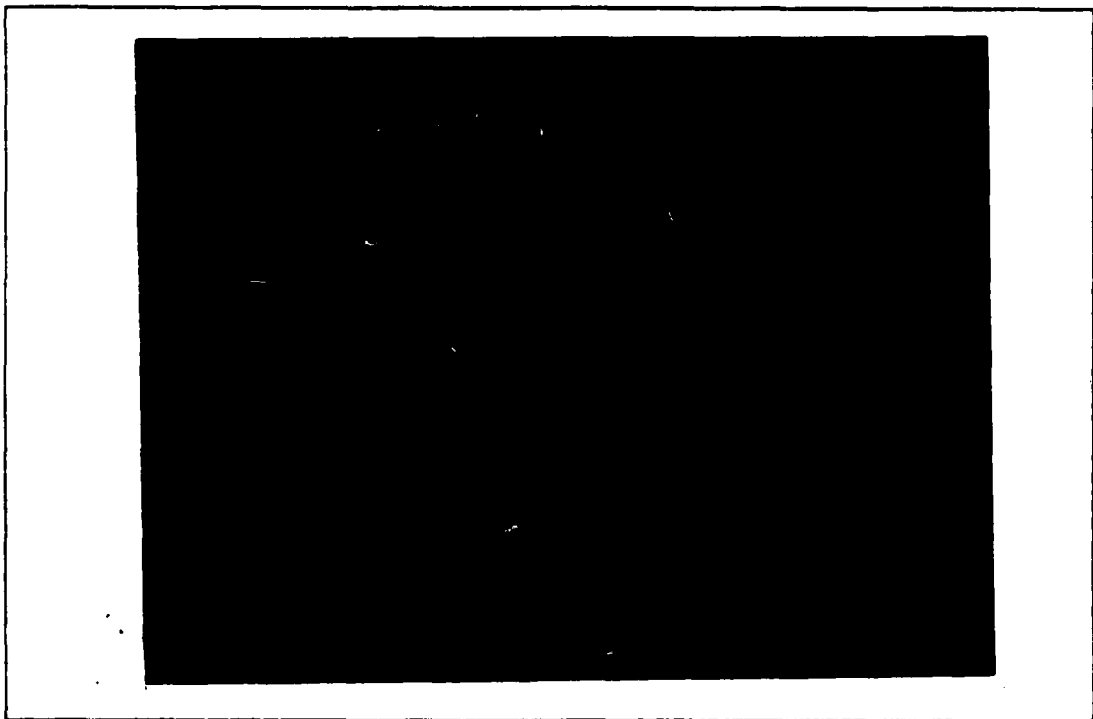


Fig. 4.5b Cloud-free channel 4 standard deviations.

The cool SST band extending southwesterly from Point Conception, as detected by channel 4 radiance measurements, does not appear in the monthly mean SST depiction, where warm water has been analyzed. However, cloud contamination is suspected in this band as implied by the radiance values detected by channels 1, 2 and 4 in the cloud-free cases, thus the disparity between the two SST analyses reinforces the contamination argument. Also, the warm mid-ocean SST anomaly is indistinguishable in the NWS mean SST analysis, but the presence of an anomaly at the same location in other cloud-free channel images indicates that this feature may yet exist.

The standard deviation depiction (Fig. 4.5b) is relatively uniform over the entire field. This should be expected with an oceanographic feature like SST since the physical processes characteristically operate under a much longer time scale than the atmosphere. However, this image can be roughly divided approximately along 40°N latitude with slightly larger variances to the north. This area is relatively close to the maximum 500 mb contour gradient along which surface disturbances tend to track. Such disturbances would disrupt the upper oceanic layers, mixing the sea-surface temperatures (Gill, 1982). Two weak frontal systems did dissipate along the northern edge of this region during the August dates as noted in Chapter III. Further support of this reasoning is provided by the indication of partial cloud contamination from the cloud-free results in this area, which is a contributing factor to higher standard deviations. Additionally, the presence of the subarctic oceanic front within this northern region would represent relatively large SST differences over a short distance by definition, and potentially significant spatial and temporal SST variances.

B. STRATOCUMULUS CLOUD CASES

1. Pixel Counts

Fig. 4.7 shows the average stratus cloud pixel counts, which are inversely correlated with the cloud-free pixel counts in Fig. 4.1. This suggests that the majority of pixels from the entire time period were classified as cloud-free or low stratocumulus cloud pixels, and that few pixels were removed from the data set due to classification as higher cloud. Therefore, the results are a fair representation of the marine stratus and pre-cloud aerosols during the late summer due to a sufficient data sample. The notable differences occur along the western edge of the images, which are easily explained through lack of data, and in the northwestern ocean area. This region of few cloud pixel counts is likely a result of the weak frontal systems that dissipated near the area

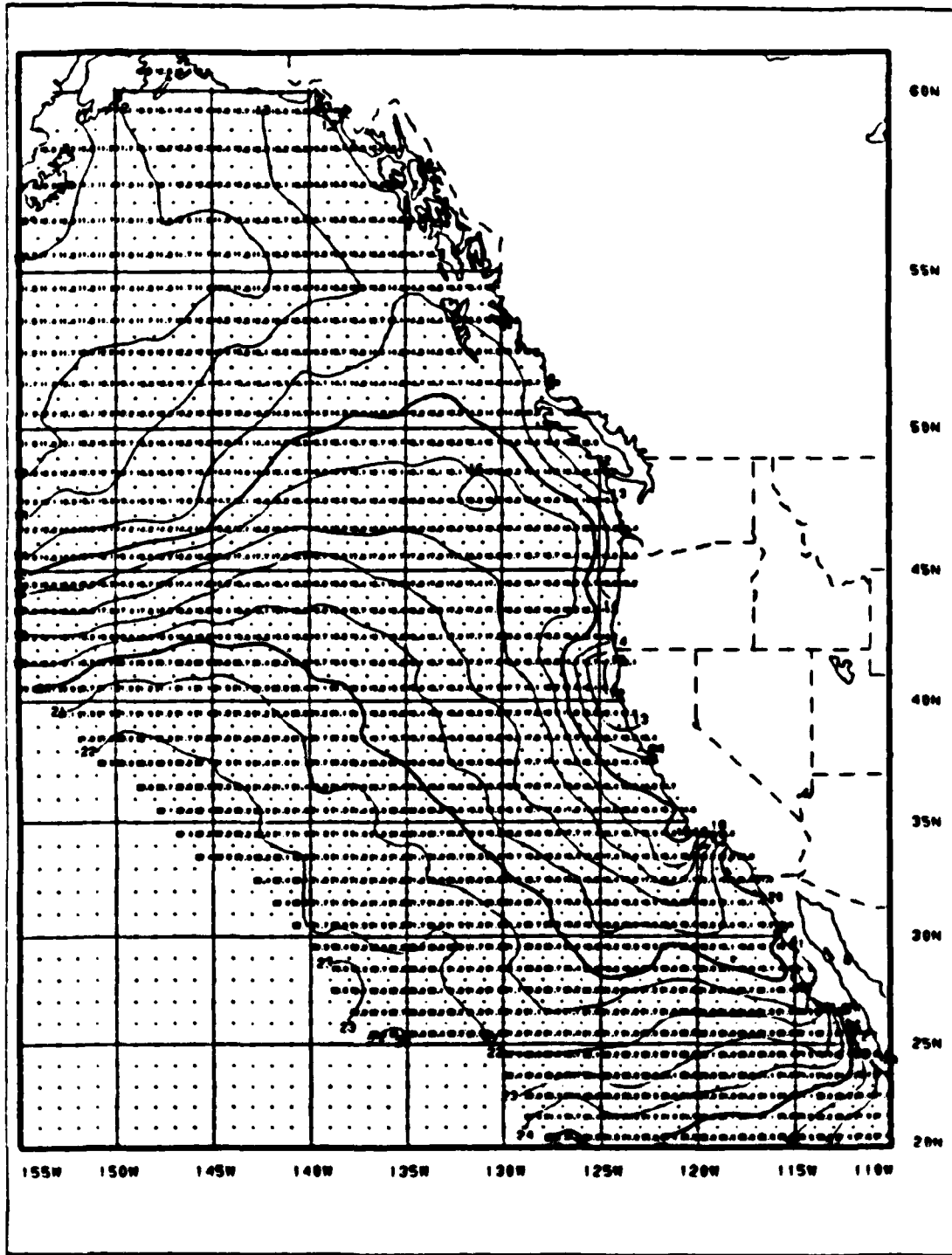


Fig. 4.6 NWS monthly mean SST for August 1986 (1.0°C interval), from Dept. of Commerce, NOAA (1986).

and the 500 mb jet flow, which would bring high clouds over the region. Clouds other than low stratocumulus were removed from the data set with the thresholding process.

A large area of stratocumulus cloudiness extends southwestward from the central California coast. The stratus in this region is climatologically significant from May through September due to a combination of geographic and atmospheric factors. Northerly air flow over coastal California is anchored by the anticyclonic circulation of the Pacific high to the west, and the cyclonic flow around a thermal low over the inland valleys and deserts to the east. As this air flows over the cold Davidson California current and the summertime upwelling of cold water depicted along the California coast in Fig. 4.5a, this air is cooled near the surface. Upper-level air on the eastern side of the subtropical high is warmed by subsidence, a characteristic of these synoptic-scale pressure centers. Thus, the air is cooled from below and warmed from above, forming a strong marine inversion. This inversion acts as a cap to the cool marine air, which quickly develops into low stratus or sometimes advection fog. The most persistent cloudy regions are located directly downwind of the coastal cold water areas as verified by extremely large stratus cloud pixel counts greater than 1390 pixels in some spots. These areas are found along the central California coast south of the upwelling near Cape Mendocino, and expanding southward past Point Conception as seen in Fig. 4.7.

The cloud-free areas include the Southern California Bight, the western coast of Vancouver Island, and the coastal and offshore region extending from the coast just north of Cape Mendocino. The clearing in these spots may be explained by various combinations of topographic clearing, land/sea breeze influences, warm SST, synoptic-scale circulations, and unique surface wind reversals as described previously in the cloud-free pixel count section of this chapter.

2. Channel 1 Reflectances

The channel 1 stratocumulus cloud reflectance averages are shown in Fig. 4.8a. A large triangular region of highly reflective clouds with values greater than 0.54 was detected along the central California coast and extending southwesterly over the ocean. This area correlates reasonably well with the area of maximum cloud pixels in Fig. 4.7, implying that the most persistent stratus has the greatest reflectance. This observation is consistent with the expectation that cloud reflectance increases at visible wavelengths with greater liquid water content and increased cloud thickness. Also, clouds with these characteristics obviously require more energy and time to dissipate than thinner clouds with a lower liquid water content.

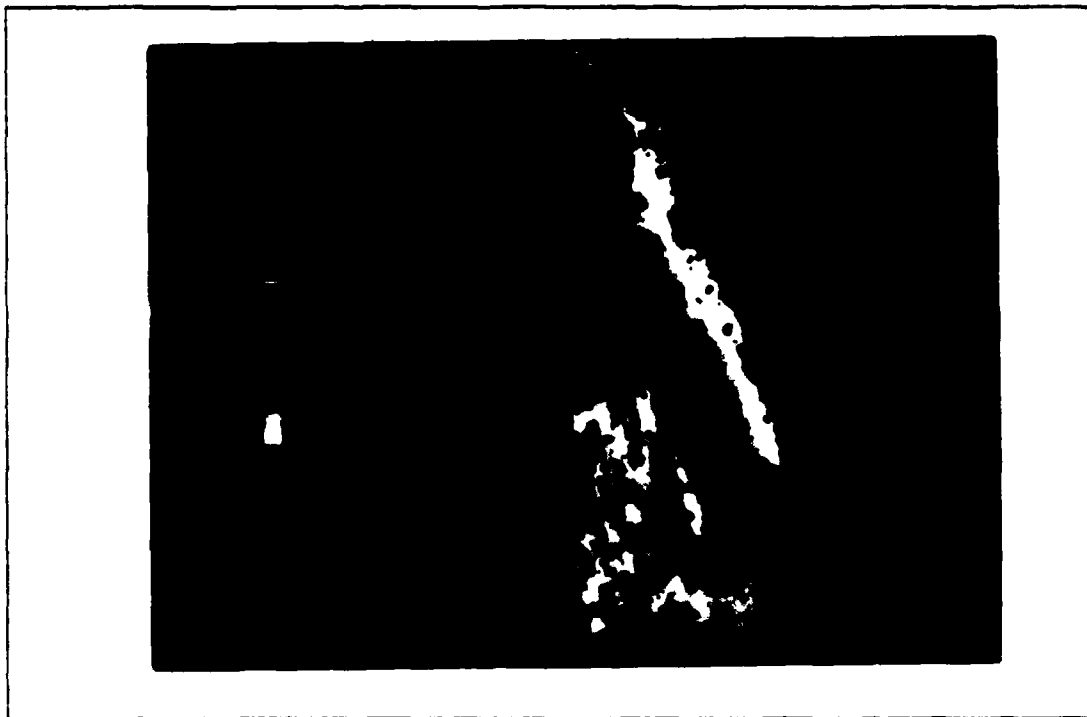


Fig. 4.7 Stratus pixel counts.

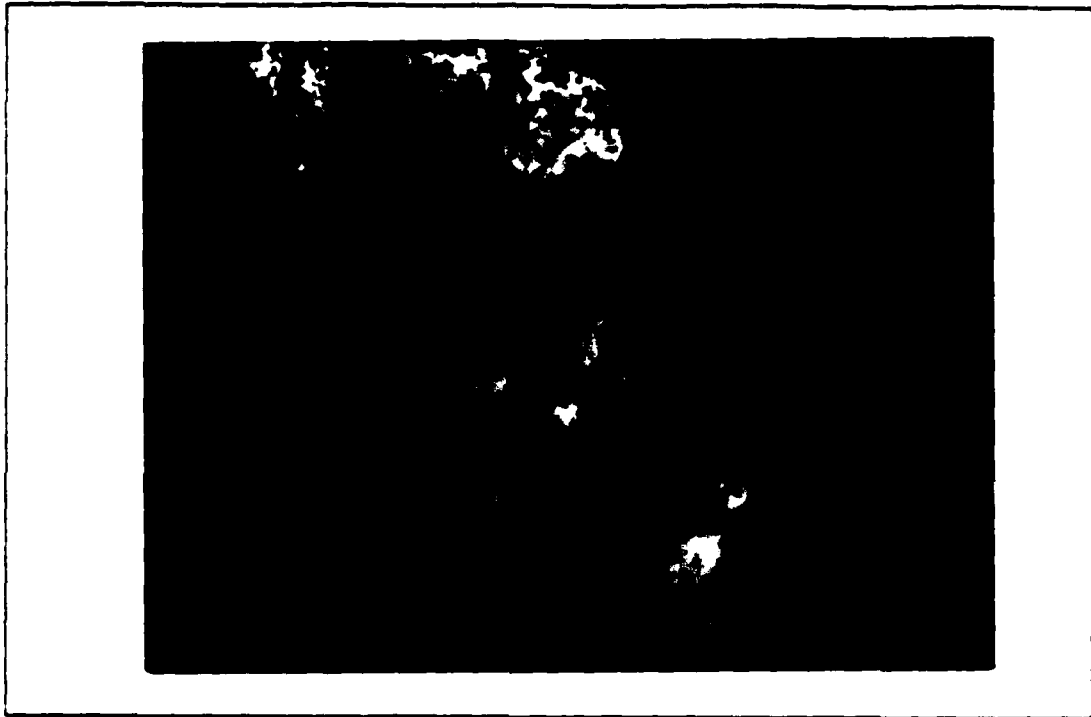


Fig. 4.8a Stratus channel 1 reflectances.

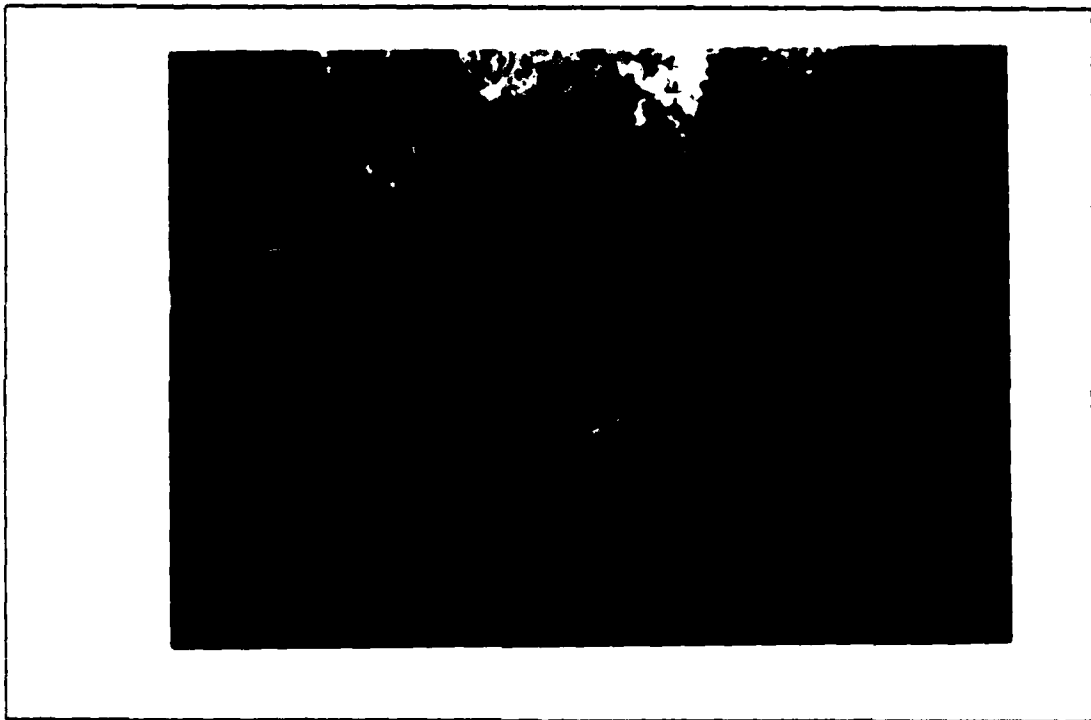


Fig. 4.8b Stratus channel 1 standard deviations.

Several factors may be responsible for the greater liquid water content and thickness of the clouds in this high reflectance region. As the northerly air flow passes over the cold coastal waters of northern and central California, the liquid water content increases through condensation and the addition of moisture from the sea surface. Continental particles make up a size distribution with smaller particles that are generally less hygroscopic than the larger sea salt particles, which would tend to form smaller droplets. However, they provide a more abundant source of CCN along the coast for cloud droplet formation and growth in correlation with the increased available liquid water as the aerosols move over water. Thus, the stratus thickens with additional cloud droplets and liquid water content. These clouds spread southwesterly over ocean waters in line with the divergent circulation around the subtropical high.

The cloud reflectance west of Vancouver Island is not as high as the reflectance described above, but it is significantly higher than the surroundings, and may also result from similar processes to those of the central California clouds. Cold water is also present along this northern coast, and the paper mills that populate this region provide an abundant source of CCN. The large standard deviations of this region, as depicted in the channel 1 cloud reflectance standard deviation image (Fig. 4.8b), with variances greater than 0.212 probably reflects the variation of cloud transport and paper mill operation.

One other notable zone of high cloud reflectance, with values again approximating 0.54, occurred in the same spot that the anomaly was detected with the cloud-free channels. It is estimated that the warm SST in this location possibly enhanced the convective activity and, therefore, the cloud thickness. The existence of small particles and possibly high CCN numbers over this spot, as implied by the results of cloud-free channel 1/channel 2 ratios in Fig. 4.4a, also may have increased the stratus thickness in the same manner as discussed above.

The cloud reflectance in the Southern California Bight is relatively low (less than 0.40). This is an indication of the low liquid water content and thin cloudiness resulting from strong evaporation caused by warm SST and strong solar heating at this latitude (Lee *et al.*, 1980). These same factors in combination with the sea breeze caused the clearing detected in the pixel count images of Fig. 4.1 and Fig. 4.7. The other significant area of average low reflectance was detected west of Cape Mendocino, but this was also a data sparse region so the stratus is likely to be thin and easily dissipated when it does develop here.

Therefore, the most revealing feature in the standard deviation image in Fig. 4.8b is the small variance along the central California coast that steadily increases southwestward in rough correlation with the high reflectance area of Fig. 4.8a. This represents the increasing variability of the stratus thickness and liquid water content as it is transported away from the cloud generation area along the coast. A small coastal spot south of Los Angeles with a reflectance value of 0.17 is also highly variable, most likely due to the differing amounts of stratus burn-off each afternoon. This area has been identified as normally cloud-free in this analysis.

3. Channel 1/Channel 2 Reflectance Ratios

As theoretically predicted, the average channel 2 stratus reflectance pattern in Fig. 4.9a matched that of channel 1 in Fig. 4.8a, and the channel 2 reflectance values were detectably lower than those of channel 1. The associated channel 2 standard deviation pattern in Fig. 4.9b also matched the respective channel 1 pattern in Fig. 4.8b, but the magnitudes in this case were larger than the channel 1 variances. These results summarily support the inferences drawn from the channel 1 stratus reflectances. An examination of the ratios between these two visible wavelength reflectances may reveal some additional information about absorptance and reflectance.

Theoretically, it is very difficult to form any concrete conclusions about the stratocumulus cloud characteristics based on the channel 1/channel 2 reflectance ratios depicted in Fig. 4.10a. The ratio values are a function of the complex relationship between cloud absorption, reflectance and transmission. However, some information can be gleaned from the ratios when Fig. 4.10a is examined in conjunction with the cloud reflectances in Fig. 4.8a and Fig. 4.9a. The distribution of the ratio values over the analyzed area is very distinctive. A triangular region of small ratios at less than 1.13 is present along the central California coast and then extends southwesterly over the ocean. It matches almost perfectly with the region of maximum visible reflectance in channel 1 and channel 2. The ratios steadily increase outward from this low ratio zone to maximums greater than 1.21 in the northwestern and southeastern corners of the analyzed area. This part of the pattern does not correlate closely to the average reflectance values of channel 1 and channel 2 as the low ratio zone does. This verifies the complexity of the Mie scattering relationship described previously between various incident radiation wavelengths and different element sizes.

The stratus in the low ratio region has been described as thick with high liquid water content based on the high channel 1 reflectance. The cloud reflectance from



Fig. 4.9a Stratus channel 2 reflectances.

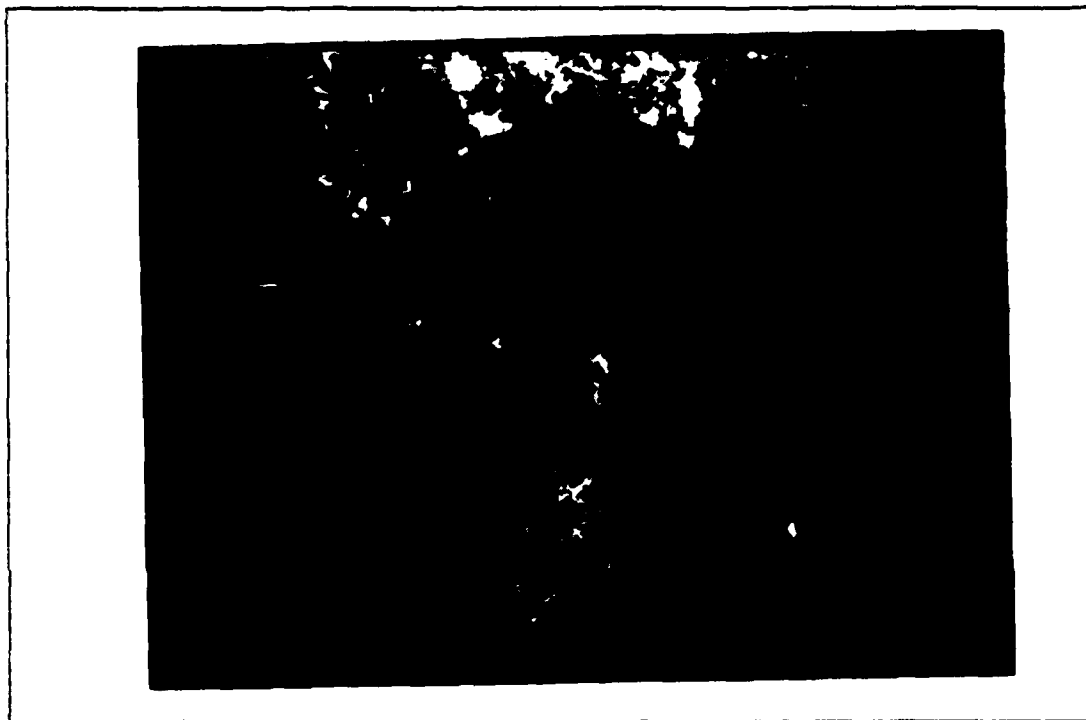


Fig. 4.9b Stratus channel 2 standard deviations.

both channels is high, which could imply that this thickness extends horizontally so that the pixels represent complete clouds or a true stratus layer. The higher ratios represent clouds with greater channel 1 reflectances than channel 2 reflectances, which could indicate partial cloudiness in the pixels as represented by regions of scattered cloud cover. This partial cloudiness argument holds up whether the channel 1 reflectances are large or small, but the layer of complete stratus would be expected only with thick, highly reflective clouds.

Fig. 4.10b shows the channel 1/channel 2 reflectance ratio standard deviations. As might be expected, the variance pattern within the low ratio region extending from central California matches those of the channel 1 and channel 2 cloud reflectances (Fig. 4.8b and Fig. 4.9b, respectively). The ratio variance outside of this low ratio zone resembles the reflectance patterns of channel 1 and channel 2 with generally higher deviations correlating to higher reflectance values in the relatively large ratio areas. This supports the partial cloud theory in that the individual clouds would move from day to day, dramatically altering the reflectances each day with the amount of cloud within a given pixel. Highly reflective clouds would show even greater variation. The mid-ocean anomaly appeared again in this stratus reflectance ratio image. It can be identified as a relatively low ratio region with values less than 1.133, which implies that the pixels represent complete cloud-covered pixels. The standard deviation in this area is distinctly low (less than 1.11) as shown in Fig. 4.10b. This may indicate that these clouds represented a single event occurrence.

4. Channel 3 Reflectances

The cloud reflectances at the near infrared wavelength of channel 3 depicted in Fig. 4.11a are more representative of the droplet size distribution and density of droplets than the liquid water content and cloud thickness, as they are at the visible wavelengths of channel 1. Based on this relationship, the channel 3 average stratus reflectances in Fig. 4.11a are as expected. The largest reflectance values at greater than 0.19 are located along the entire California coast, indicative of a large number of cloud water droplets formed from a continental-like CCN size distribution. The maximum reflectance spot with a value greater than 0.24 is found just south or downwind of Los Angeles, which could result from stratus formed from the local urban pollution. The particle size distribution of these urban aerosols is often strongly weighted toward small particles, and pollutants are usually concentrated in large numbers. These two characteristics in the stratus that form would increase the cloud reflectance in channel

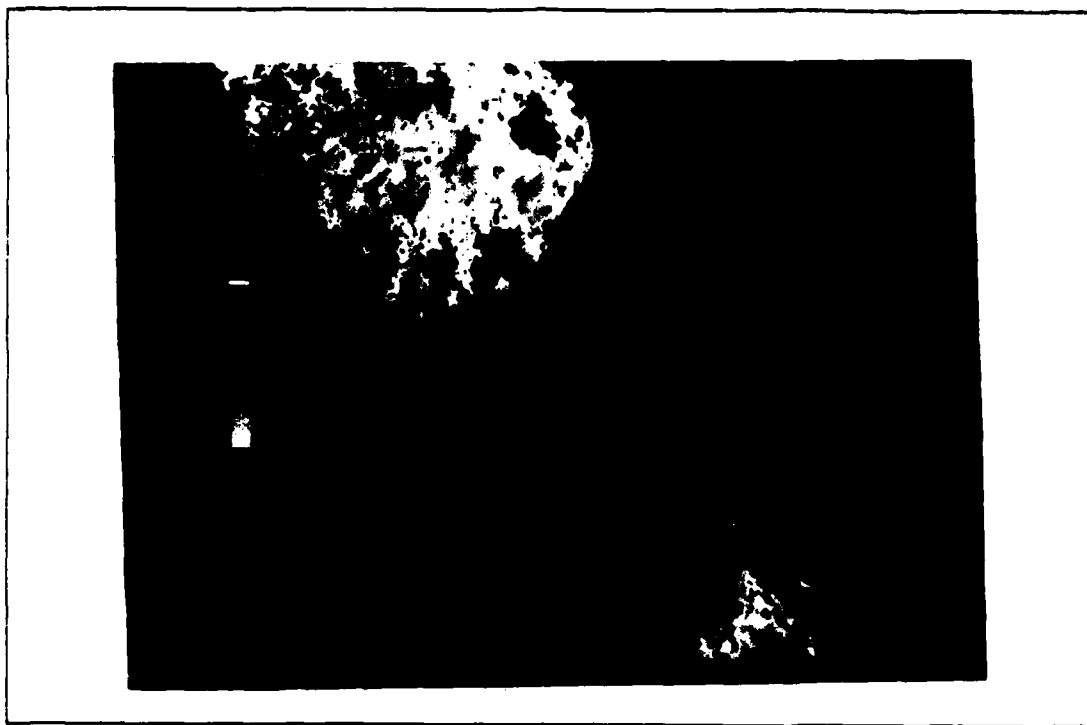


Fig. 4.10a Stratus channel 1/channel 2 reflectance ratios (x 100).



Fig. 4.10b Stratus channel 1/channel 2 ratio standard deviations.

3. A different type of pollutant, paper mill exhaust, may provide the CCN which develop into the relatively high reflectance values (approximating 0.12) of clouds around Vancouver Island. The cloud reflectances are not as great as those along the California coast primarily due to the more favorable conditions for cloud formation along the southern coastline in California. The synoptic-scale flow around the Pacific high transports highly reflective clouds southwesterly from the central and southern California coastline, although continental CCN characteristics tend to slowly dissipate as the clouds move away from the particle source and over the ocean.

The low reflectance stratus is located offshore near the center of the subtropical high with values less than 0.11. The clouds that develop (this is an area of small cloud pixel counts from Fig. 4.7) are probably formed from marine-like particle size distributions, which are weighted toward large particles. The relatively larger droplets that result are less reflective than smaller droplets of continental origin at this near infrared wavelength. Smaller numbers of cloud droplets are also responsible for the lower reflectances. Fewer aerosols to act as CCN are suspended in air due to the characteristically light winds and subsidence near the center of high pressure circulations. All of these factors may contribute to make high pressure centers relatively cloud-free.

The cloud-free ratios of channel 1 to channel 2, depicted in Fig. 4.4a, provide information concerning suspended aerosol number and size distributions in cloud-free atmospheric conditions. These pre-cloud particle characteristics can be linked to the stratocumulus clouds as classified by these channel 3 reflectance values. Clouds composed of continental CCN are slightly downwind of the continental aerosols and generally expansive with respect to the synoptic-scale flow. This is illustrated by suspended aerosols along the coast in Fig. 4.4a and then continental-like stratus from Cape Mendocino expanding southerly along the coast into the Southern California Bight and over the southwestern ocean area. The channel 1/channel 2 reflectance ratio maximums along the central California coastline and near Los Angeles correspond to the channel 3 stratus reflectance maximums in the same regions. Marine-like stratus appears near the subtropical high in connection with relatively low cloud-free ratio values that represent marine aerosols. The high ratio anomaly can also be correlated to an area of relatively high cloud reflectance in channel 3.

The standard deviations of the channel 3 cloud reflectances are displayed in Fig. 4.11b. The pattern of variances corresponds roughly to these reflectances, which



Fig. 4.11a Stratus channel 3 reflectances.

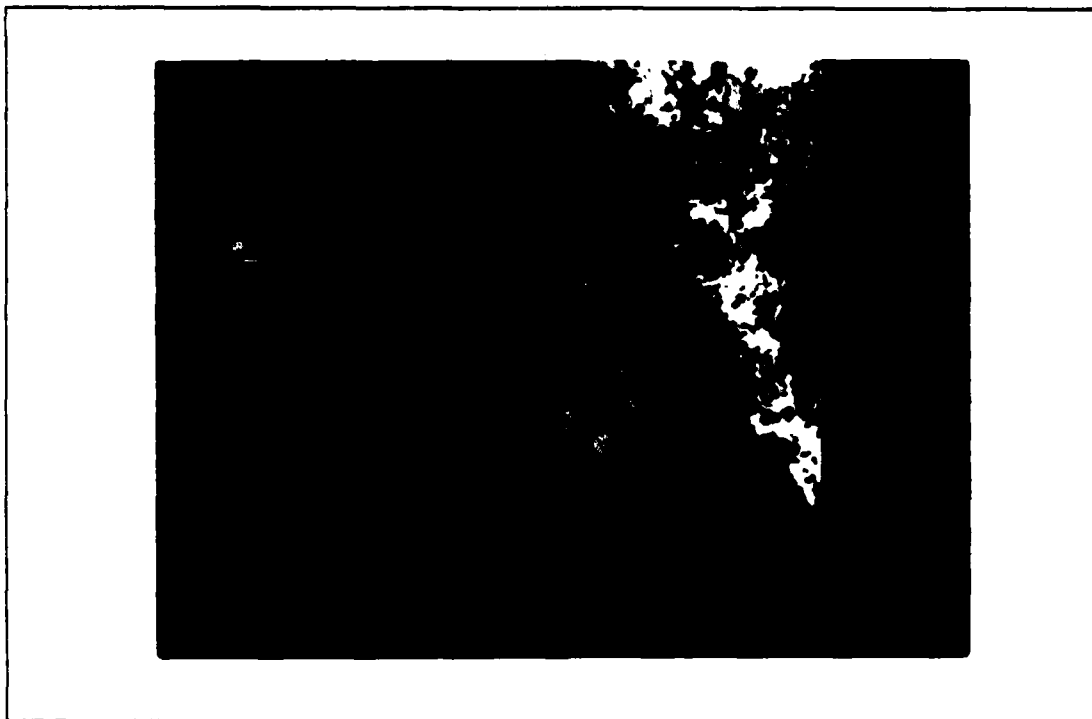


Fig. 4.11b Stratus channel 3 standard deviations.

suggests that stratus composed of numerous droplets formed from continental CCN have more variable near infrared reflectance characteristics than the clouds formed by fewer droplets with maritime CCN size distributions. The southern section of the Southern California Bight differs from this correlation as the deviations are small despite the indication that the stratus has a continental-like origin. However, lack of data in this region is not responsible for the apparent aberration.

5. Channel 1/Channel 3 Reflectance Ratios

The ratio of visible to near infrared cloud reflectances, depicted in Fig. 4.12a, is indicative of multiple cloud characteristics. Low reflectance areas such as the entire Southern California Bight south of Point Conception and the large region just offshore northern California are theoretically representative of the continental-like stratus with ratio values approximately less than 2.50. This type of cloud is relatively thin and dry from a low liquid water content, which would be reflected in a low channel 1 value. These clouds are also composed of many smaller droplets resulting from a continental size distribution of CCN, which would increase the channel 3 reflectance and further decrease the channel 1, channel 3 ratio. This class of stratocumulus cloud would be expected in the Southern California Bight with the warm shallow water and strong latitudinal solar radiation to dry out the clouds and the nearby coastline to provide a source of continental CCN. In fact, the entire North American coast should therefore exhibit some continental-like stratus characteristics, and the relatively low ratio (approximately 2.50) along the coast does support this conclusion. However, the low reflectance ratio area off northern California appears to be rather unusual. The cloud data in this spot are sparse from Fig. 4.7, and the area shows up as a distinct cloud-free zone from the pixel counts in Fig. 4.1. The low ratio values may represent the contribution of a very low channel 1 reflectance resulting from thin dissipating clouds.

The reflectance ratios steadily increase westwardly over the Pacific Ocean from the coast. These higher ratios represent marine-like stratus that may have a higher liquid water content than the continental-like stratus. The cloud droplets are generally fewer in number and originate from a maritime particle size distribution of CCN. This type of stratocumulus is reasonable over water away from the continent.

The standard deviations for these reflectance ratios are shown in Fig. 4.12b. Interestingly, the stratus ratios along the entire continental coastline had the lowest standard deviations with their respective small ratio values. The least deviation occurred along the southern California coast where the smallest ratios also appeared,



Fig. 4.12a Stratus channel 1/channel 3 reflectances ratios (x 100).



Fig. 4.12b Stratus channel 1/channel 3 ratio standard deviations.

although the variance did increase slightly into the bight. One other distinctively small variance area is located just offshore from central California in a region roughly similar to the unusually small ratio area noted previously. The multiple factors influencing these standard deviations make it difficult to draw any reliable conclusions. For example, small deviations may actually represent extremely high near infrared (channel 3) variances or very low visible (channel 1) variances, whereas large standard deviations may represent low near infrared variances or high visible variances.

6. Channel 4 Temperatures

Fig. 4.13a displays the average cloud-top temperatures from thermal infrared cloud emittances. The colder cloud tops with temperatures less than 282.0 K like those across the northern section, in the southwest corner and along the northern to central California coast indicate either generally higher cloud tops due to higher inversion heights or clouds within a colder air mass. The cold cloud-top temperatures along the coastal regions correlate with the cold SST and upwelling event detected in Fig. 4.5a, implying that these temperatures represent a relatively cold air mass rather than a high inversion cap. The small minimum temperature spot at 282.0 K just north of Cape Mendocino interestingly correlates very closely with the cloud-free pixel maximum in Fig. 4.1. Thus, the low cloud tops indicated by very warm temperatures (greater than 286.0 K) in the Southern California Bight would result from the orographic subsidence downwind of the Arguello headland. The easy detection of islands in the bight, represented by the absolute temperature maximums, supports the low stratus argument in this region as the stratus layer sits below the island peaks (450 m). Climatologically, this northern versus southern coastal inversion height difference is typical of the summertime situation.

The lower stratocumulus cloud tops implied by the warm temperatures in the central Pacific Ocean also occur in the maximum subsidence region of the subtropical high. The other two areas of implied higher cloud tops occur away from the high pressure center. These colder temperatures are also present in regions of small stratus pixel counts from Fig. 4.7.

The standard deviations associated with the cloud-top temperatures are depicted in Fig. 4.13b. The maximum variance areas correspond roughly to the high cloud tops in the northern and southwestern sections around the Pacific high, and the low stratus region in the Southern California Bight. The variable heights of the coastal stratus south of Los Angeles is probably due to the different sea breeze strengths each

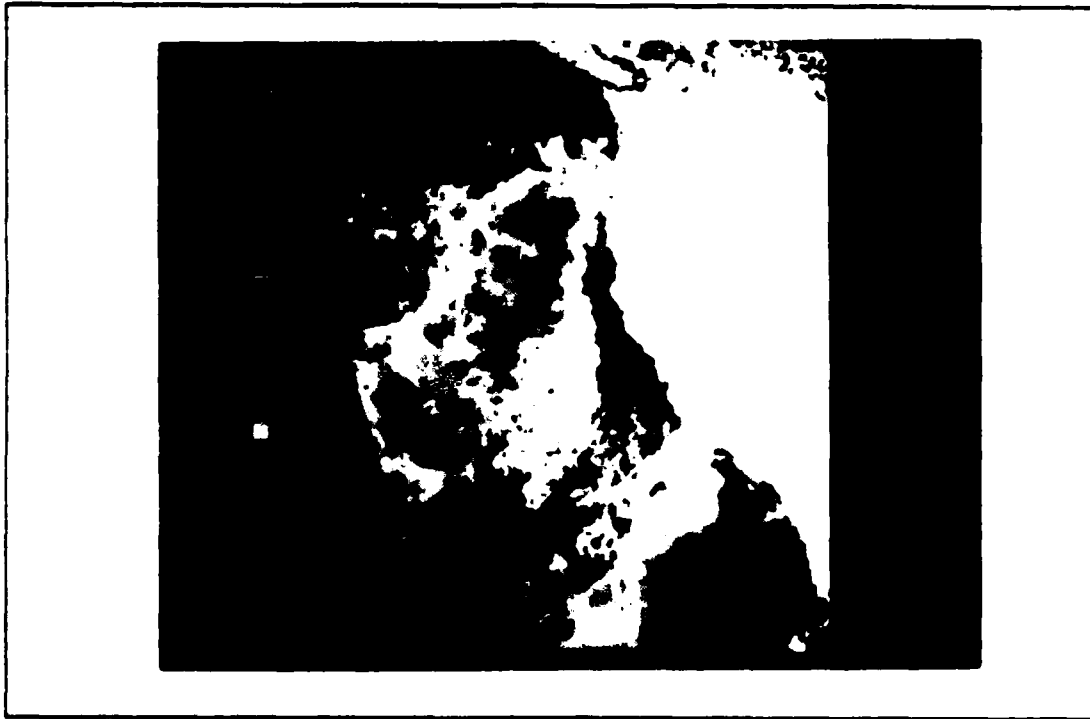


Fig. 4.13a Stratus channel 4 temperatures.

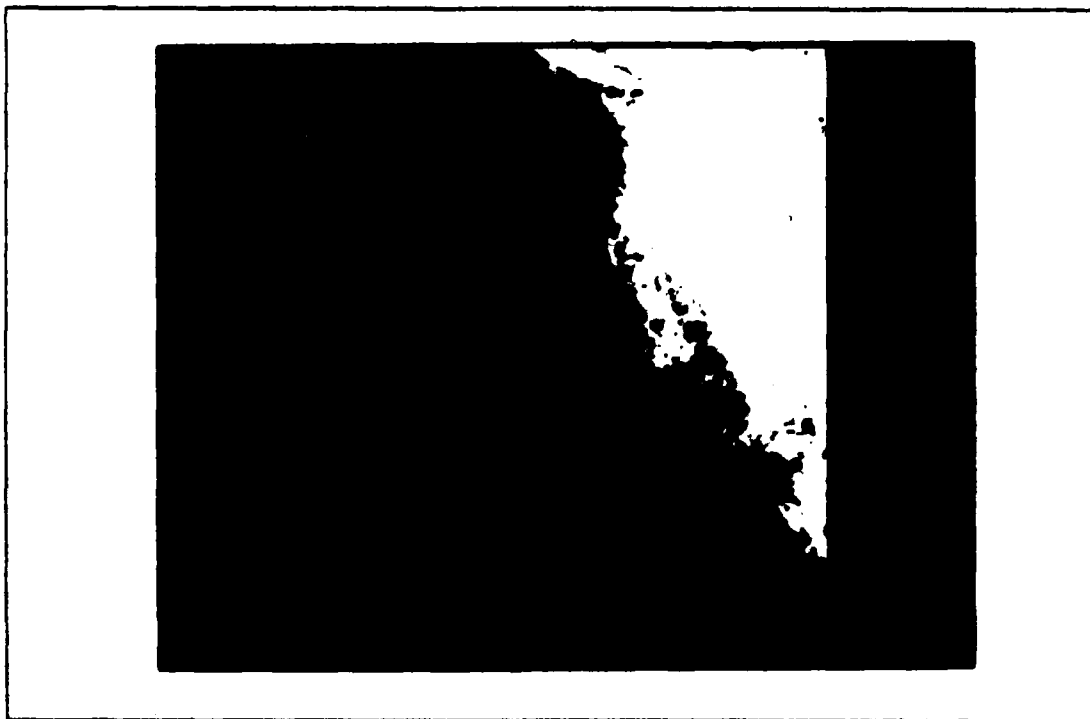


Fig. 4.13b Stratus channel 4 standard deviations.

afternoon, which affect the amount of stratus dissipated near the coast. The other two regions represent the effects of a small data sampling. The subsidence region underneath the high pressure center is also cloud data sparse, but the low cloud tops show little variability. The United States west coast and offshore areas north of Los Angeles show small deviations, which also infer relatively consistent inversion heights. The persistence of the stratus may account for this relatively small variability.

V. CONCLUSION

A. SUMMARY

Backscattered and emitted radiance data collected by the five-channel AVHRR onboard the NOAA-9 satellite was evaluated over eighteen dates in August and early September of 1986. The analysis covered the eastern north Pacific Ocean and west coast of the North American continent in a 25° by 25° square grid. This area was further divided into 0.1° by 0.1° individual boxes, approximately 10 pixels by 10 pixels, to calculate the average radiances and standard deviations. Each pixel was subjected to threshold tests in order to categorize it as cloud-free or low stratocumulus cloud. All other pixels (mid-level or high cloud) were eliminated from evaluation.

The multi-channel capability of the AVHRR was utilized to create several different analysis fields. The channel 1 and channel 2 reflectances were evaluated along with the ratios of the two reflectances. The channel 4 emittances were converted to temperatures for analysis. These temperatures were also used to calculate an estimation of channel 3 emittance. These emittances were then subtracted from the total radiance measured by channel 3 to estimate the channel 3 reflectances. Reflectance ratios between channel 1 and channel 3 were also computed. An anisotropic reflectance adjustment (ARF) was incorporated into each of the reflectance values in the stratocumulus cloud cases to account for variations due to sun-earth-satellite geometry.

Thus, a composite summary of multi-spectral radiative characteristics from the visible, near infrared and infrared portion of the electromagnetic spectrum was created for the cloud-free ocean and marine stratocumulus clouds in late summer 1986 over the eastern North Pacific Ocean. Several significant features with plausible explanations were identified from this summary:

1. Coastal concentrations of small-sized (less than $1 \mu\text{m}$) aerosols were derived from the channel 1/channel 2 reflectance ratios in cloud-free data images. High ratio values approximating 1.70 or greater imply the presence of small particles in relatively large numbers. These particles are characterized as continental-like aerosols composed of silicates and carbon. Extremely high ratios approaching 2.13 were calculated downwind of urban centers like San Francisco Bay and Los Angeles. These ratios represent additional particles of increasingly smaller size, which may indicate possible pollutants. The lower ratio values were calculated

from the reflectances detected over mid-ocean areas, implying the presence of fewer particles of generally larger size (greater than 1 μm). These larger particles probably represent sea salt from the ocean and are classified as marine-like aerosols.

2. Stratocumulus cloud reflectance ratios from channel 1 and channel 3 were representative of several cloud characteristics which were correlated to the pre-cloud aerosols described above. Lower reflectance ratios imply relatively thin, dry stratus from a low liquid water content (lower channel 1 reflectances) and a greater number of smaller cloud droplets (higher channel 3 reflectances). The properties define stratus of roughly continental (CCN) origin. Such clouds correlate closely with the continental-like aerosols as the stratus was generally downwind of these particles, along the entire U.S. west coast especially over the Southern California Bight and offshore from northern California with ratio values less than 2.50. Stratus of marine (CCN) origin, defined by a higher channel 1 channel 3 reflectance ratio (greater than 3.50) indicating moist clouds of generally fewer, but larger droplets, was located over the mid-ocean areas. Available marine-like aerosols were also detected by cloud-free channel 1 channel 2 reflectance ratios over the oceanic regions.
3. SST mapping from channel 4 emittance measurements illustrated a significant coastal cold water (283.0 K to 285.5 K) upwelling event north of Cape Mendocino. This cold water extended southward along the central California coast as evidence of the Davidson California current. Very warm SST (greater than 291.0 K) were detected along the coastal boundary and southern portion of the Southern California Bight. Such temperatures indicated additional solar heating of these relatively cloud-free areas.
4. Areas of persistent coastal clearing were identified from the cloud-free pixel summations. A maximum cloud-free zone with 1200 pixels was located along the coast north of Cape Mendocino with an extensive clear area expanding offshore. This unique phenomenon was correlated with small-scale wind reversal forcing (Dorman, 1987). Another persistent clearing maximum (1100 cloud-free pixels) was defined along the northeastern coast of the Southern California Bight, centered near Los Angeles. This cloud-free area was linked to topographic clearing and sea breeze effects.
5. A persistent stratocumulus cloud concentration was defined by stratus pixel summations along the central California coast and extending offshore with the synoptic-scale flow around the Pacific high pressure center to the southwest. Pixel counts within this large stratus layer exceeded 900 pixels. The region was further defined by radiation measurements in different AVHRR channels. These included a channel 1 reflectance maximum greater than 0.54, implying the possible effects of thick stratus clouds with a high liquid water content. The channel 3 reflectance values in this region were greater than 0.16 and increased toward a maximum of 0.22 near the coast, implying a droplet number increase also toward the coast. The cool channel 4 cloud-top temperature measurements (less than 284.0 K) indicated that this stratus was in a cold air mass, influenced

by the coastal upwelling and cold SST identified by cloud-free channel 4 measurements.

Additionally, some interesting and unexpected features also appeared as a result of these multi-spectral radiative measurements. These intriguing results include:

1. An offshore anomalous region defined by a very low cloud-free Channel 1 reflectance (0.035), a high cloud-free channel 1 channel 2 reflectance ratio (greater than 200.0) and relatively warm SST (greater than 290.0 K) from cloud-free channel 4 temperatures. These measurements infer that the area contained a small number of suspended aerosols (channel 1 reflectance) with a size distribution weighted toward smaller particles (less than 1 μm from channel 1 channel 2 reflectance ratio). It was hypothesized that these aerosols may have been of oceanic origin, specifically sulfate particles released into the atmosphere through chemical reactions from phytoplankton (Charlson *et al.*, 1987). This feature also appeared as a relative maximum (0.54) in the stratocumulus cloud channel 1 reflectances, implying a thicker cloud of higher liquid water content over this area than over the surrounding areas.
2. An extremely high cloud-free channel 1/channel 2 reflectance ratio band along the central California coast, exceeding 213.0 at its maximum. Such a large ratio value implies a large number of suspended aerosols with a size distribution weighted toward generally smaller particles. As a result of this implication and the region's proximity to (directly downwind of) the San Francisco Bay area, the ratio potentially indicates a significant occurrence of pollution.
3. A stratocumulus cloud channel 1/channel 2 reflectance ratio pattern, composed of a triangular region of minimum ratio values (less than 1.13) along the central California coast and extending southwesterly over the ocean, then decreasing steadily outward from this area to maximums (greater than 1.21) in the northwestern and southeastern corners of the analysis area. The stratus ratio pattern is very distinctive and unique. It was hypothesized that the ratios may correlate to the amount of cloud within a pixel, lower ratios representing complete clouds or a stratus layer and the higher ratios representing partial cloudiness or individual clouds.

B. RECOMMENDATIONS

A few areas for improvement were identified during the computation process and review of the results. Based on the explainable and unexpected results summarized previously and these possible improvements, the following recommendations are suggested:

- perform case studies on the features identified in the summary

- investigate further the unexpected results described in the summary, and the causes of these unique radiative characteristics
- use *in situ* measurements of stratocumulus cloud and cloud-free properties to enhance the data, such as provided by the FIRE experiment
- use a more sophisticated clear versus cloud discrimination routine to eliminate cloud contamination as identified in the cloud-free cases
- apply a process that eliminates sunglint, but also retains data within affected area that is not contaminated by sunglint

Multi-spectral AVHRR data from the NOAA-9 satellite has been utilized to create a monthly summary of the radiative characteristics of marine stratocumulus clouds and cloud-free oceanic areas. From a careful examination of these detected radiation values and their relative magnitudes through ratios, significant features have been identified. Of special interest is the relationship of pre-cloud aerosols (from cloud-free regions) to stratus clouds. This type of information has important application to military operations and climatic calculations. Militarily, the complex sensors of many current weapon systems are highly sensitive to the electro-optical properties defined by this summary. Climatically, the earth's radiation budget is responsive to the aerosol and cloud effects on incoming solar radiation. A summary such as this provides information for estimating the contribution of these atmospheric elements to the budget calculations.

LIST OF REFERENCES

- Allen, R.C., Jr., 1987: Automated satellite cloud analysis: A multispectral approach to the problem of snow cloud discrimination. M.S. thesis, Naval Postgraduate School, Monterey, CA, 113 pp.
- Charlson, R.J., J.E. Lovelock, M.O. Andreae, and S.G. Warren, 1987: Oceanic phytoplankton, atmospheric sulphur, cloud albedo and climate. *Nature*, **326**, 655-661.
- Coakley, J.A., Jr., R.L. Bernstein, and P.A. Durkee, 1987: Effect of ship-track effluents on cloud reflectivity. *Science*, **237**, 1020-1022.
- Dorman, C.E., 1987: Possible role of gravity currents in northern California's coastal summer wind reversals. *J. Geophys. Res.*, **92**, 1497-1506.
- Durkee, P.A., 1987: Aerosol characteristics inferred from dual-wavelength radiance measurements, submitted manuscript to *J. Geophys. Res.*, May 1987.
- Fett, R.W. and R.G. Isaacs, 1979: Concerning cause of 'anomalous gray shades' in DMSP visible imagery. *J. Appl. Meteor.*, **18**, 1340-1352.
- Fleagle, R.G. and J.A. Businger, 1980: *An Introduction to Atmospheric Physics (Second Edition)*. Academic Press, Inc., Orlando, FL, 432 pp.
- Gerald, C.F. and P.O. Wheatley, 1984: *Applied Numerical Analysis (Third Edition)*. Addison-Wesley Publishing Co., Inc., Reading, MA, pp. 191-196.
- Gill, A.E., 1982: *Atmosphere-Ocean Dynamics (International Geophysics Series)*. Academic Press, Inc., Orlando, FL, 662 pp.
- Hunt, G.E., 1973: Radiative properties of terrestrial clouds at visible and infra-red thermal window wavelengths. *Quart. J. R. Met. Soc.*, **99**, 346-369.
- Kidwell, K.B., 1986: *NOAA Polar Orbiter Data Users Guide*. U.S. Department of Commerce, Washington, DC.
- Lauritson, L., G.J. Nelson, and F.W. Porto, 1979: Data extraction and calibration of TIROS-N/NOAA radiometers. NOAA Technical Memorandum NESS 107, U.S. Dept. of Commerce, Washington, DC, Appendix B.
- Lee, T.F., J. Rosenthal, and R.A. Helvey, 1980: Coastal stratus phenomena observed by GOES satellite. *Conference on Coastal Meteorology (Second)*, Los Angeles, CA, American Meteorological Society, pp. 271-281.
- Liou, K.N., 1980: *An Introduction to Atmospheric Radiation*. Academic Press, Inc., Orlando, FL, 392 pp.

- Nieburger, M., J.G. Edinger, and W.D. Bonner, 1971: *Understanding Our Atmospheric Environment*. W. H. Freeman and Company, San Francisco, CA, 293 pp.
- Ruff, I. and A. Gruber, 1983: Multispectral identification of clouds and earth surfaces using AVHRR radiometric data. *Preprints Fifth Conf. on Atmospheric Radiation, American Meteorological Society*, Baltimore, MD, 31 October - 4 November 1983.
- Shettle, E.P. and R.W. Fenn, 1979: Models for the aerosols of the lower atmosphere and the effects of humidity on their optical properties. *Tech. Rep. AFGL-TR-79-0214*, Air Force Geophys. Lab., Hanscomb Air Force Base, MA.
- Taylor, V.R. and L.L. Stowe, 1984: Atlas of reflectance patterns for uniform earth and cloud surfaces (NIMBUS-7 ERB--61 Days). NOAA Tech. Rep. NESDIS-10, U. S. Dept. of Commerce, Washington, DC, 66 pp.
- Twomey, S., 1977: The influence of pollution on the shortwave albedo of clouds. *J. Atmos. Sci.*, **34**, 1149-1152.
- U.S. Department of Commerce, National Oceanic and Atmospheric Administration, 1986: *Oceanographic Monthly Summary*, **6**, August, p. 16.

INITIAL DISTRIBUTION LIST

		No. Copies
1.	Defense Technical Information Center Cameron Station Alexandria, VA 22304-6145	2
2.	Library, Code 0142 Naval Postgraduate School Monterey, CA 93943-5002	2
3.	Chairman (Code 63Rd) Department of Meteorology Naval Postgraduate School Monterey, CA 93943-5000	1
4.	Chairman (Code 68Co) Department of Oceanography Naval Postgraduate School Monterey, CA 93943-5000	1
5.	Professor Philip A. Durkee (Code 63De) Department of Meteorology Naval Postgraduate School Monterey, CA 93943-5000	10
6.	Professor Carlyle H. Wash (Code 63Wx) Department of Meteorology Naval Postgraduate School Monterey, CA 93943-5000	1
7.	LT Fredrick M. Tettelbach, USN USS Saipan (LHA-2) OA Division FPO New York, NY 09549-1605	2
8.	Director Naval Oceanography Division Naval Observatory 34 th and Massachusetts Avenue NW Washington, DC 20390	1
9.	Commander Naval Oceanography Command NSTL Station Bay St. Louis, MS 39522	1

- | | | |
|-----|----------------------------------------------------------------------------------------------------------------------------------------|---|
| 10. | Commanding Officer
Naval Oceanographic Office
NSTL Station
Bay St. Louis, MS 39522 | 1 |
| 11. | Commanding Officer
Fleet Numerical Oceanography Center
Monterey, CA 93943-5005 | 1 |
| 12. | Commanding Officer
Naval Ocean Research and Development Activity
NSTL Station
Bay St. Louis, MS 39522 | 1 |
| 13. | Commanding Officer
Naval Environmental Prediction Research Facility
Monterey, CA 93943 | 1 |
| 14. | Chairman, Oceanography Department
U. S. Naval Academy
Annapolis, MD 21402 | 1 |
| 15. | Chief of Naval Research
800 North Quincy Street
Arlington, VA 22217 | 1 |
| 16. | Office of Naval Research (Code 420)
Naval Ocean Research and Development Activity
800 North Quincy Street
Arlington, VA 22217 | 1 |
| 17. | Scientific Liason Office
Office of Naval Research
Scripps Institution of Oceanography
La Jolla, CA 92037 | 1 |
| 18. | Dr. Paul Twitchell
Code 1244
Office of Naval Research
800 North Quincy Street
Arlington, VA 22217-5000 | 1 |

END

DATE

FILMED

8-88

OTIC